Supplementary Information for

Heteronuclear Pt^{II}-Pd^{II} Dimers Formation through Ligands Subtle Tailoring

Peng Fan, †[a] Lequn Yuan, †[a] Yuzhen Zhang *[a]

[a] Key Laboratory of Chemistry and Engineering of Forest Products, State Ethnic Affairs Commission, Guangxi Key Laboratory of Chemistry and Engineering of Forest Products, Guangxi Collaborative Innovation Center for Chemistry and Engineering of Forest Products, School of Chemistry and Chemical Engineering, Guangxi Minzu University, Nanning, Guangxi 530006, China

* Corresponding author. E-mail: zhangyuzhen@gxmzu.edu.cn

Contents

1. Materials

All commercially available starting materials were used directly without further purification. All solvents were purchased from standard suppliers and were be used without further purification. Before conducting photoluminescence (PL) and electroluminescence (EL) properties investigations, all final products were dried to further improve purity. Flash column chromatography was performed employing 200-300 mesh silica gel. Thin layer chromatography (TLC) was performed on silica gel.

2. Instrumentation

NMR: ^{1}H and ^{13}C NMR spectra were all recorded on Bruker 400 spectrometers in acetone-d_6 at room temperature. ^{195}Pt NMR spectra were all recorded on JEOL 600 MHz spectrometers in chloroform-d at room temperature. The following abbreviations are used to describe the multiplicity of signals: s (singlet); d (bimodal); t (triplet); dd (doublet of doublet); m (multimodal).

High-resolution MS data were recorded using ThermoFisher Scientific (USA) equipped with an electrospray ionization source (ESI). Accurate mass determination was corrected by calibration using sodium trifluoroacetate clusters as a reference.

UV−Vis absorption measurements were carried out on an Agilent Cary 100 UV−Vis spectrophotometer.

Emission spectrum, phosphorescence lifetime and quantum yield were measured directly using Edinburgh Instruments model FLS1000. Emission spectra were acquired using xenon lamp excitation by exciting at the longest-wavelength absorption maxima with the excitation slit width 1.0 nm and emission slit width 1.0 nm. Absolute quantum yields and phosphorescent lifetimes were measured in neat crystalline state, PMMA (Polymethylmethacrylate) films and solution of dichloromethane using an integrating sphere on the Edinburgh spectrophotometer FLS1000 at room temperature. Samples were N_2 degassed by more than three freeze-pump-thaw cycles before measurement. The PL lifetimes were extracted from the resulting decay curves by performing exponential fitting and deconvolution with the instrument response function. The photophysical rate constants for radiative decay (k_r), non-radiative decay (k_{nr})were calculated according to the literature equations[1]: $\phi(PLQY)=k_r\times\tau$; $\tau=1/(k_r+k_{nr})$.

PMMA film: Mix the complex with polymethyl methacrylate (PMMA) in a mass ratio. After mixing evenly, used a dropper to take a little of the above solution and drop it evenly on quartz glass. After drying, a PMMA film containing sample can be obtained to measured its photophysical properties.

Cyclic voltammogram were performed on CHI760e (manufactured by CH Instruments, Inc)

with a solution of tetra-n-butylammonium hexafluorophosphate (*n*-Bu_4NPF_6, 0.1 M) in MeCN as electrolyte and ferrocene/ferrocenium (Fc^+/Fc) as an internal standard. A three-electrode configuration (Ag^+/Ag, platinum wire and glassy carbon electrode as the reference, counter, and working electrodes, respectively) was used in CV measurements. The ionization potential (E_{HOMO}) of the compounds were determined from the half-wave potential relative to that of Fc^+/Fc using the equation E_{HOMO} [eV] = -(E_{ox}' + 4.8) eV [2]. Where, the energy level of LUMO (E_{LUMO}) was calculated with the equation E_{LUMO} [eV] = E_{HOMO} + E_g. E_{ox}' represent the onset oxidation potentials relative to Fc^+/Fc, to measure the onset oxidation potential (E_{onset}), using the tangent of the CV peak, and the formula E_{ox}' = E_{onset} - $E_{1/2ferrocene}$. Estimations were done with the empirical relation $E_{1/2ferrocene}$ = (E_{pc} + E_{pa}) / 2, E_{pc} and E_{pa} represent the oxidation and reduction potentials of ferrocene, respectively[3] [4]. The longest absorption wavelength λ_{onset} was used to calculate the optical gap energy, E_g, according to the equation: $E_g = hc/\lambda_{onset}$. Where h is Planck's constant, λ_{onset} is compound absorption onset, and c is the speed of light in vacuum. Note that none of the samples have reduction peaks.

X-ray data collection and structure determination. Crystals suitable for X-ray diffraction analysis were obtained by slow evaporation of dichloromethane from the hexane-dichloromethane mixture. The experiments were carried out using Agilent Technologies single crystal diffractometer with CCD area detectors and Oxford Cryosystems open-flow cryostats. Using graphite monochromatic MoK_α rays, at a certain temperature, within a certain range of θ, the diffraction point data of the crystal is collected. Data were corrected for absorption using multiple-scan method or numerical integration based on actual crystal shape. The structures were solved by ShelXS6 and refined by full-matrix least squares using Olex-2 software and use ShelXL7 for optimization. When mixing and adding hydrogen, hydrogen atoms use isotropic thermal parameters, and non-hydrogen atoms use anisotropic thermal parameters. The thermal ellipsoids were drawn at the 30% probability level. Hydrogen atoms were omitted for clarity. The corresponding CCDC reference number (CCDC: 2311651 and 2311650) and the data can be obtained free of charge from the Cambridge crystallographic data center via www.ccdc.cam.ac.uk/. Their crystal data are listed on **Table S1, 2, 3**.

Resonance Raman Spectra were recorded on Renishaw inVia QONTOR (micro-confocal Raman spectrometer) by using the excitation wavelength of 785 nm.

Thermogravimetric analysis (TGA) was carried out on Perkin-Elmer Pyris Diamond TG starting from room temperature (25 ℃) to 800 ℃ at a heating rate of 10 ℃/min in a N_2 atmosphere.

OLED device configuration: Pre-patterned indium tin oxide (ITO) coated glass (10 Ω sq^{-1}) was used as an anode substrate and was carefully cleaned before use. Organic and metallic

materials were grown in a vacuum chamber below 1.0×10^{-5} Pa, respectively. The evaporation rate of HAT-CN in the hole injection layer was controlled at 0.01 nm s-1, and that of TAPC in the hole transport layer was controlled at 0.05 nm s^{-1}. When evaporating the luminescent layer, the luminescent material and the host material were evaporated simultaneously from different sources, and the evaporation rate of the host material was controlled at 0.05 nm s^{-1}, and the evaporation rate of the luminescent material was adjusted according to the difference in doping concentration. The evaporation rate of Tm3PyP26PyB in the electron transport layer was controlled at 0.05 nm s^{-1}. The evaporation rates of LiF and Al were controlled at 0.01 nm s^{-1} and 0.5 nm s^{-1}, respectively. All the devices were characterized without encapsulation at room temperature. The current density-voltage-luminance (J-V-L) characteristics, EQE, CIEx, y, and EL spectra of the devices were measured using the M6100 OLED IVL test system.

3. Synthetic Procedures

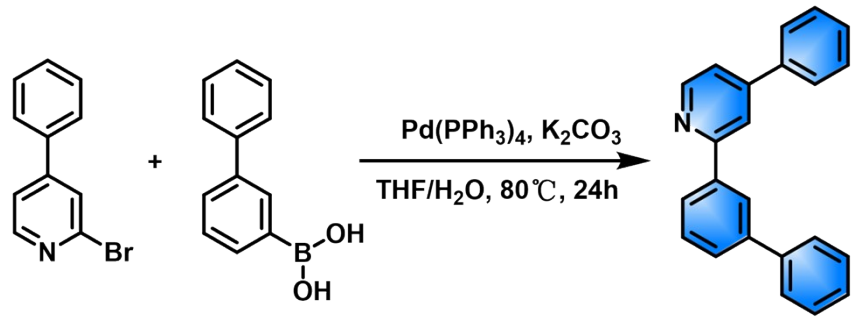

Figure S1. General procedure for synthesis of 2-[(1,1 '- biphenyl)-3-yl]-4-phenylpyridine.

Complex 2-[(1,1 '- biphenyl)-3-yl]-4-phenylpyridine was prepared according to a pub lished procedure[5]. An oven-dried Schlenk tube was charged with 2-bromo-4-phenyl-py ridin (250mg,1.07mmol), Biphenyl-3-boronic acid (253mg,1.28mmol), $Pd(PPh_3)_4$ (61mg,0. 053mmol) and K_2CO_3 (442mg,3.20mmol) in nitrogen atmosphere. Dry THF was then a dded and the reaction mixture was stirred 80℃ for 24 hrs. The reaction was quenc hed with water (5 mL) and removing all the solvents by rotary evaporation, CH_2Cl_2 was added. The organic layer was separated, washed with water, dried over MgSO4, filtered, and evaporated to dryness. And the residue was purified with silica gel colu mn chromatography using the eluent of DCM/*n*-hexane. 211 mg white solid was obt ained (yield: 64%).

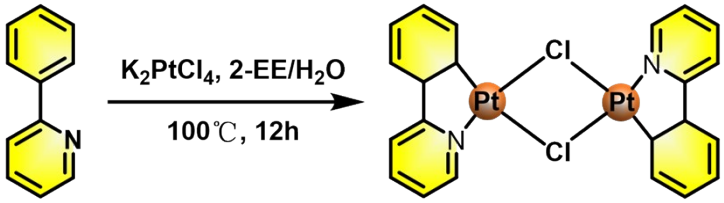

Figure S2. General procedure for synthesis of $[Pt(ppy)Cl]_2$ (P1).

Complex $[Pt(ppy)Cl]_2$ was prepared according to a published procedure[6]. To a mixt ure of 2-Phenylpyridine (100 mg, 0.64 mmol) and K_2PtCl_4 (267 mg, 0.64 mmol) was added the mixture of 2-Ethoxyethanol (2-EE) (8 mL) water (1 mL). The mixture was reacted at 100 ℃ for 12 h. After cooled to RT, add a large amount of water to pr

ecipitate solids, the precipitate was filtered and washed with water, diethyl ether. We obtained yellow green solid (218 mg, 87%). This product was used for the next step directly without further purification.

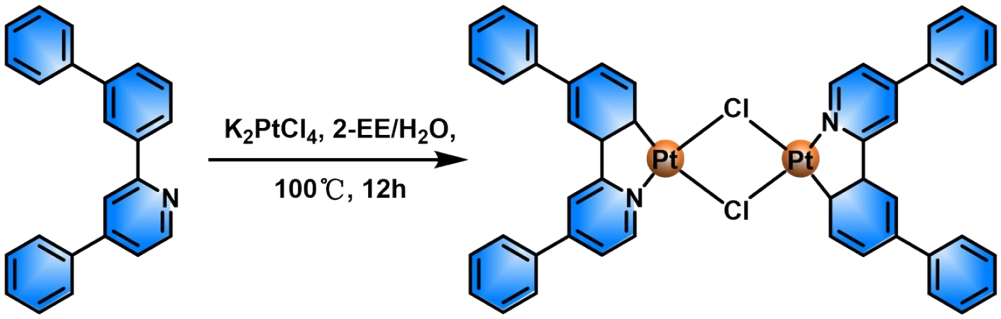

Figure S3. General procedure for synthesis of $[Pt(bppy)Cl]_2$ (P2).

Following a similar procedure as described for $[Pt(ppy)Cl]_2$, using 2-[(1,1 '- biphenyl)-3-yl]-4-phenylpyridine (148 mg, 0.48 mmol), $[Pt(bppy)Cl]_2$ (130 mg, 57%) was isolated as a light green solid. This product was used for the next step directly without furt her purification.

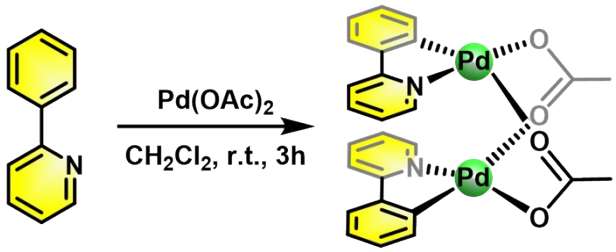

Figure S4. General procedure for synthesis of $[Pd(OAc)(ppy)]_2$ (P4).

Complex $[Pd(OAc)(ppy)]_2$ was prepared according to a published procedure[7]. To a solution of 2-phenylpyridine (186 mg, 1.20 mmol) in CH_2Cl_2 (24 mL) at 23℃ is added palladium acetate (268 mg, 1.20 mmol). After stirring for 3 h, the orange solution is concentrated in vacuo. wash solid with ether, we obtained orange-yellow solid (287 mg, 74%). This product was used for the next step directly without further purification.

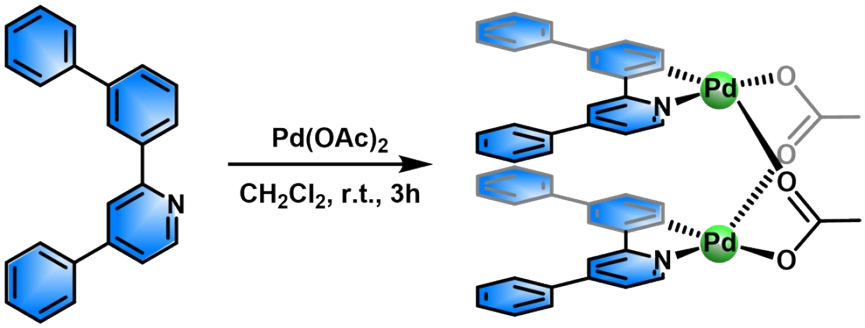

Figure S5. General procedure for synthesis of $[Pd(OAc)(bppy)]_2$ (P3).

Following a similar procedure as described for $[Pd(OAc)(ppy)]_2$, using 2-[(1,1 '- biph enyl)-3-yl]-4-phenylpyridine (200 mg, 0.65 mmol), $[Pd(OAc)(bppy)]_2$ (60 mg, 60%) was isolated as a yellow solid. This product was used for the next step directly without further purification.

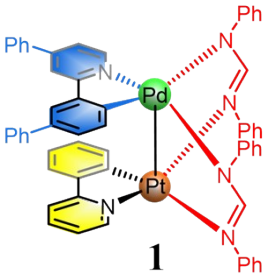

Figure S6. Structure of **1.**

An oven-dried Schlenk tube was charged with $[Pt(ppy)Cl]_2$ (40mg, 0.052mmol), $[Pd(OAc)(bppy)]_2$ (49mg, 0.052mmol), *N,N'*-diphenylformamidine (HDPhF) (51mg, 0.26mmol) and K_2CO_3 (34mg, 0.26mmol) in nitrogen atmosphere. Dry 1,2-Dichloroethane (DCE) and a small amount of deionized water was then added and the reaction mixture was stirred in the dark at 90 ℃ for 24 hrs. The reaction was quenched with water (5 mL) and removing all the solvents by rotary evaporation, CH_2Cl_2 was added. The organic layer was separated, washed with water, dried over MgSO4, filtered, and evaporated to dryness. And the residue was purified with silica gel column chromatography using the eluent of DCM/*n*-hexane. 29 mg red solid was obtained (yield: 24%). This reaction will simultaneously generate two synuclear byproducts, $[Pt (bppy) (HDPhF)]_2$ and $[Pd (ppy) (HDPhF)]_2$, in addition to the target product. They will display yellow, red (target product), and deep red on the TLC plate (developer, *n*-hexane: dichloromethane=3:2) from high to low. It has been verified that using a small amount of solvent (1,2-dichloroethane) to participate in the reaction will preferentially generate by-products $[Pt (bppy) (HDPhF)]_2$, while using a large amount of solvent will preferentially generate the target product.

^{1}H NMR (400 MHz, Acetone-d6, 23 °C) δ 8.44 (s,1H), 8.17 (s, 1H), 7.79 (d, 1H), 7.75 (m, 3H),

7.69 (m, 6H), 7.58 (m, 8H), 7.47 (m, 6H), 7.34 (m, 7H), 7.13 (m, 8H), 6.88 (m, 3H), 6.49 (dd, 1H), 6.13 (t, 1H);

^{13}C NMR (100 MHz, Acetone-d6, 23 °C): δ 167.83, 165.62, 161.89, 161.28, 158.02, 153.05, 152.65, 152.48, 152.24, 151.59, 149.87, 147.12, 142.55, 138.48, 137.77, 137.06, 135.94, 134.08, 130.31, 129.97, 129.92, 129.60, 129.50, 129.37, 129.22, 129.08, 128.07, 128.01, 127.50, 127.45, 125.42, 125.18, 124.69, 124.01, 123.84, 123.62, 123.60, 123.08, 122.80, 122.71, 122.68, 121.72, 119.66, 118.48, 116.54, 64.74, 32.65, 30.74, 23.34, 14.36.

^{195}Pt NMR (600 MHz, Chloroform-d, 23 °C): δ -3179.00.

HR-MS (ESI): m/z calcd. for $C_{60}H_{46}N_6PtPd$ $[M+H]^+$: 1152.2539; Found: 1152.2565.

Elemental analysis: Calc for $C_{60}H_{46}N_6PtPd$: C, 62.53%; H, 4.02%; N, 7.29%; found: C, 62.46%; H, 3.629%; N, 7.34%.

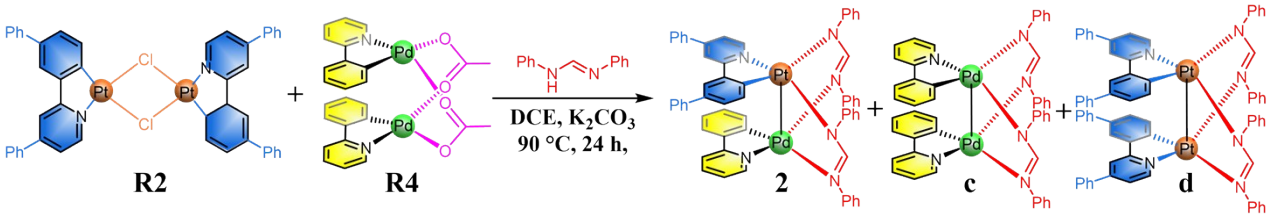

Figure S7. Structure of **2.**

Following a similar procedure as described for **1**, using $[Pd(OAc)(ppy)]_2$ (20mg, 0.031 mmol), $[Pt(bppy)Cl]_2$ (34mg, 0.031mmol), *N,N'*-Diphenylformamidine(31mg, 0.16mmol), K_2CO_3 (22mg, 0.16mmol), **2** (22 mg, 31%) was isolated as a red solid. As long as a large amount of solvent is used in this reaction, only the target product will be generated without any by-products, and only one red luminescent point will be displayed on the TLC board.

^{1}H NMR (400 MHz, Acetone-d6, 23 °C): δ 8.43 (s, 1H), 8.17 (s, 1H), 7.77 (m, 4H), 7.66 (m, 8H), 7.54 (m, 6H), 7.47 (m, 5H), 7.33 (m, 8H), 7.12 (m, 8H), 6.88 (m, 3H), 6.45 (dd, 1H), 6.15 (t, 1H).

^{13}C NMR (100 MHz, Acetone-d6, 23 °C): δ 167.79, 165.65, 161.87, 161.33, 158.52, 153.06, 152.68, 152.45, 152.31, 151.71, 151.45, 149.66, 146.72, 146.63, 142.95, 138.45, 137.98, 135.87, 135.68, 134.52, 130.35, 130.00, 129.61, 129.49, 129.46, 129.32, 129.27, 129.16, 128.59, 128.00, 127.29, 127.20, 125.15, 124.75, 124.03, 123.85, 123.81, 123.62, 123.53, 123.17, 123.12, 122.80, 121.74, 119.69, 118.48, 116.52, 32.31, 23.29, 14.35.

^{195}Pt NMR (600 MHz, Chloroform-d, 23 °C): δ -3156.92.

HR-MS (ESI): m/z calcd. for $C_{60}H_{46}N_6PtPd$ $[M+H]^+$: 1152.2539; Found: 1152.2537.

Elemental analysis: Calc for $C_{60}H_{46}N_6PtPd$: C, 60.81%; H, 3.96%; N, 7.03%; found: C, 61.06%; H, 3.593%; N, 6.92%.

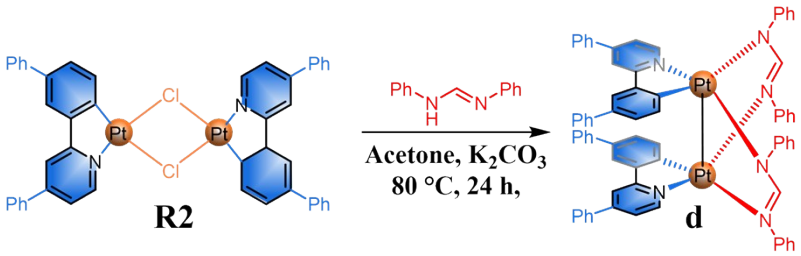

Figure S8. Structure of **d.**

Due to the optimization of experimental conditions, by-products **c** and **d** were not separated during the synthesis of complex **2**. As our research group has already synthesized **c** and conducted relevant characterization, d has never been synthesized. We synthesized d to investigate the property differences between complex **2** and **c** and **d**.

The dichloro-bridged intermediate $[Pt(bppy)Cl]_2$ (100 mg, 0.093 mmol), *N,N'*-diphenylformamidine (40 mg, 0.20 mmol), K_2CO_3 (13 mg, 0.093 mmol), acetone 20 mL and 1ml H_2O were into a Schlenk flask and stirred at reflux condition under nitrogen atmosphere for 24 h. After cooling down to room temperature, the solvent was removed. The residue was extracted with CH_2Cl_2. The organic fraction was collected and dried with $MgSO_4$. After the filtration, the solvent was removed and the crude product was purified by silica column chromatography with eluent of DCM/*n*-hexane. Red solid 13 mg, 10% yield.

^{1}H NMR (400 MHz, CD_2Cl_2, 23 °C): δ 8.47 (d, 2H), 7.69 (d, 4H), 7.665 (d, 2H), 7.58 (d, 4H), 7.49 (dd, 2H), 7.41 (m, 28H), 7.17 (m, 6H), 7.09 (t, 2H), 6.93 (t, 2H), 6.92 (dd, 2H).

^{13}C NMR (100 MHz, CD_2Cl_2, 23 °C): δ 166.85, 160.44, 151.83, 151.23, 151.09, 149.00, 145.65, 145.32, 141.97, 137.58, 135.26, 133.99, 129.80, 129.48, 129.17, 128.89, 128.80, 128.31, 127.21, 126.85, 126.70, 124.71, 123.96, 123.13, 123.03, 121.75, 119.15, 115.24.

HR-MS (ESI): m/z calcd. for $C_{72}H_{54}N_6Pt_2$ [M]: 1391.3679; Found: 1391.3693.

4. Photophysical Properties

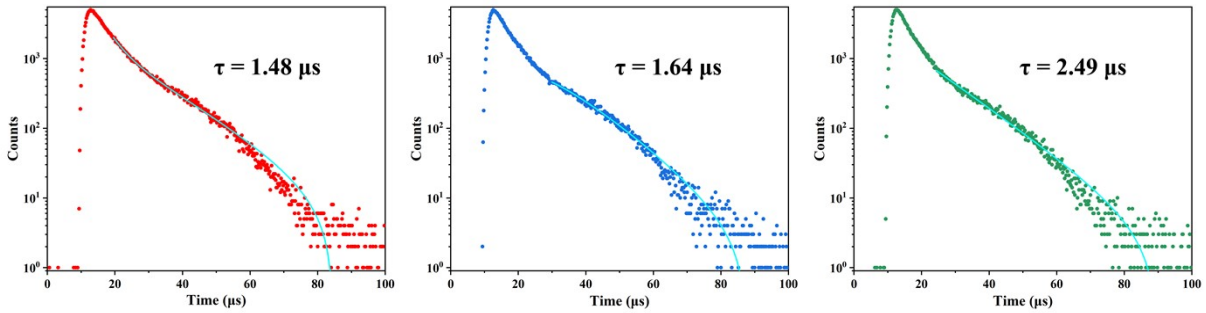

Figure S9. PL decay curves of complex **1** in different concentrations of PMMA (1wt%, 10wt%, 20wt% from left to right).

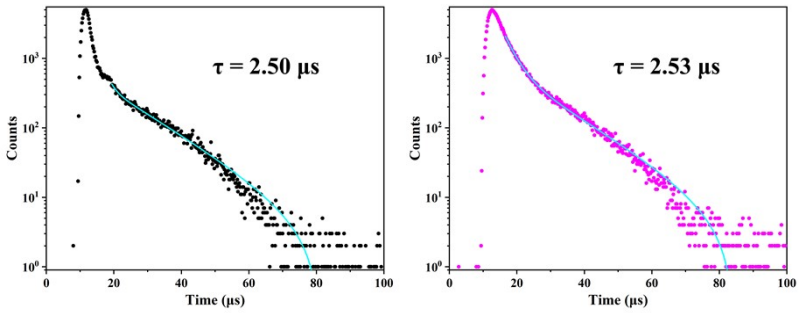

Figure S10. PL decay curves of **1** in air-free CH_2Cl_2(black) at room temperature and neat crystalline state (magenta).

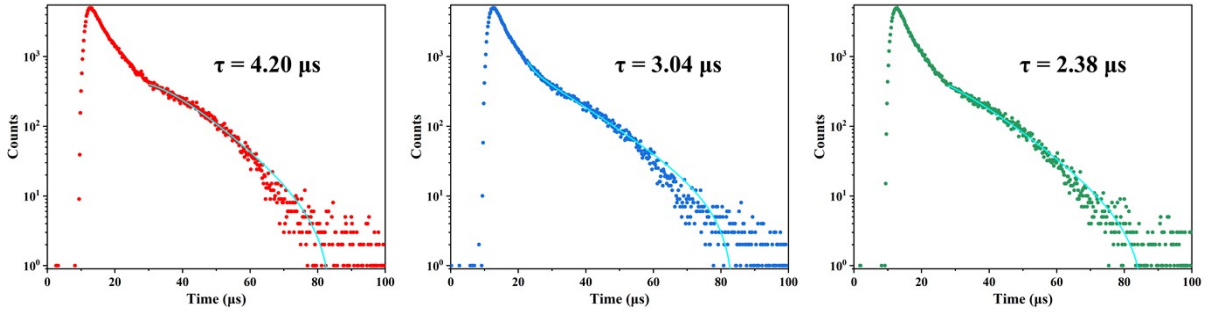

Figure S11. PL decay curves of **2** in different concentrations of PMMA (1 wt.%, 10 wt.%, 20 wt.% from left to right).

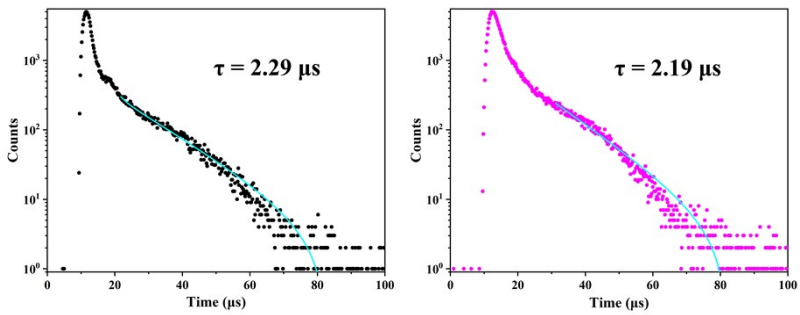

Figure S12. PL decay curves of complex **2** in air-free CH_2Cl_2(black) at r.t. and crystalline state (magenta).

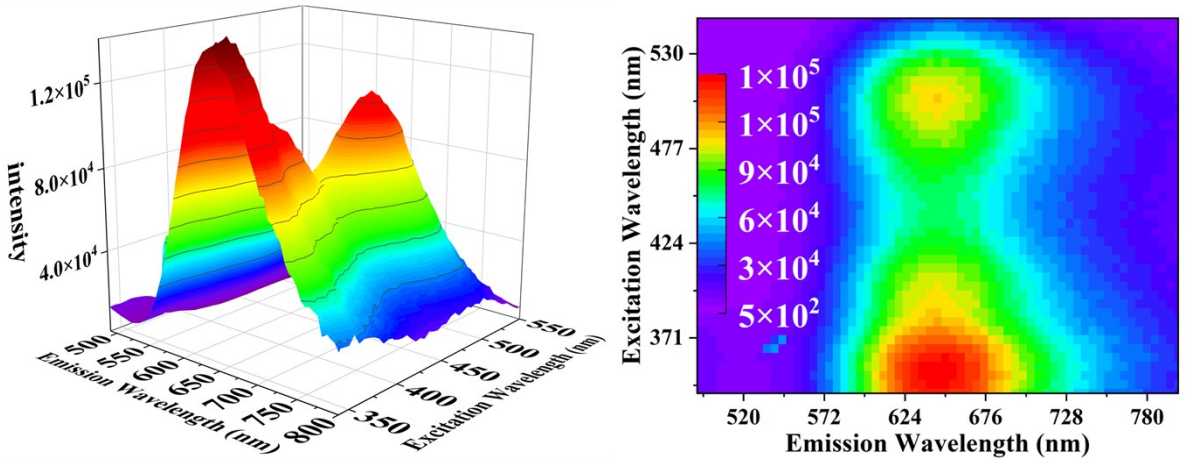

Figure S13. Excitation-dependent emission spectra in 2 wt. % PMMA film of **1** (Left: 3D Stereoscopic View, Right: 2D Planar View).

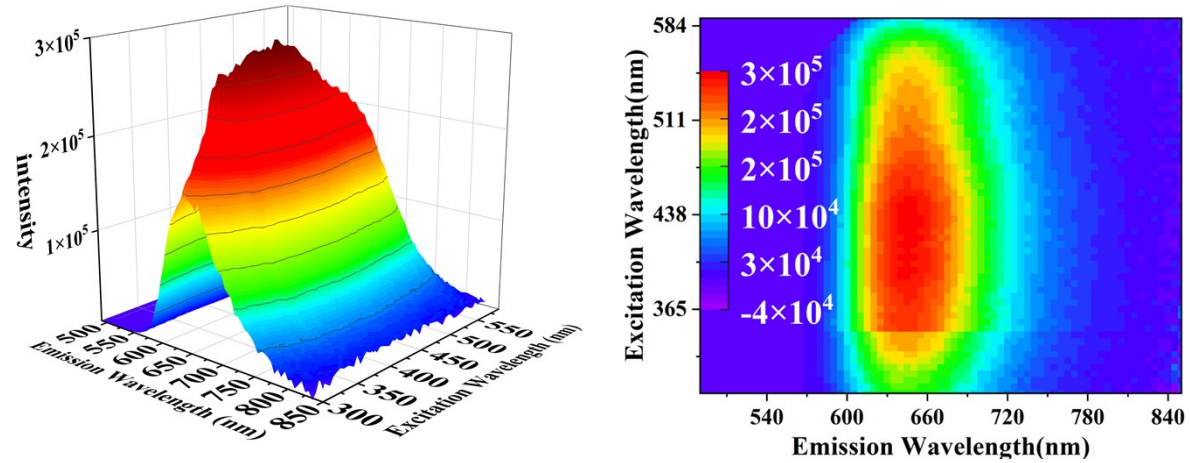

Figure S14. Excitation-dependent emission spectra of **1** in crystalline state at room temperature (Left: 3D Stereoscopic View, Right: 2D Planar View).

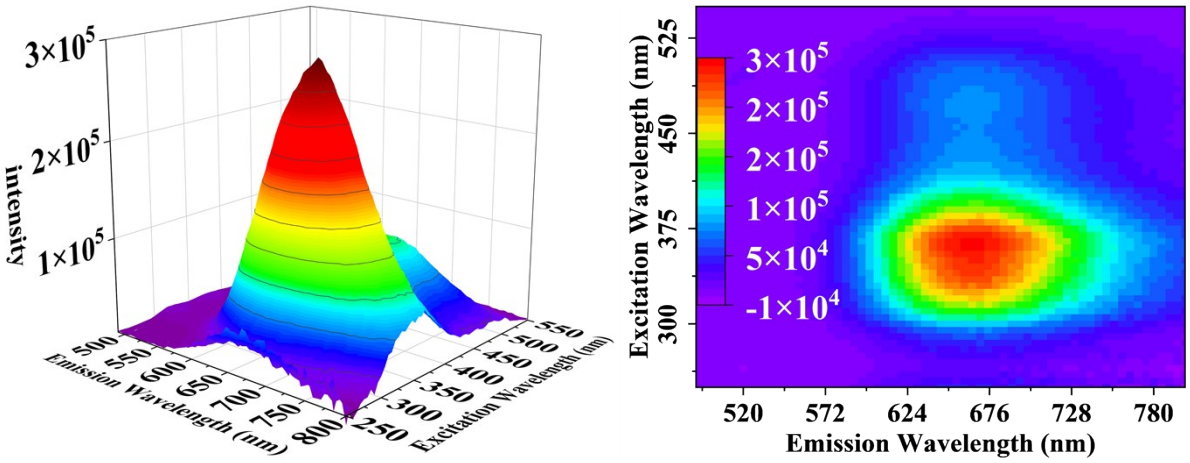

Figure S15. Excitation-dependent emission spectra of **1** in air free CH_2Cl_2 at room temperature (Left: 3D Stereoscopic View, Right: 2D Planar View).

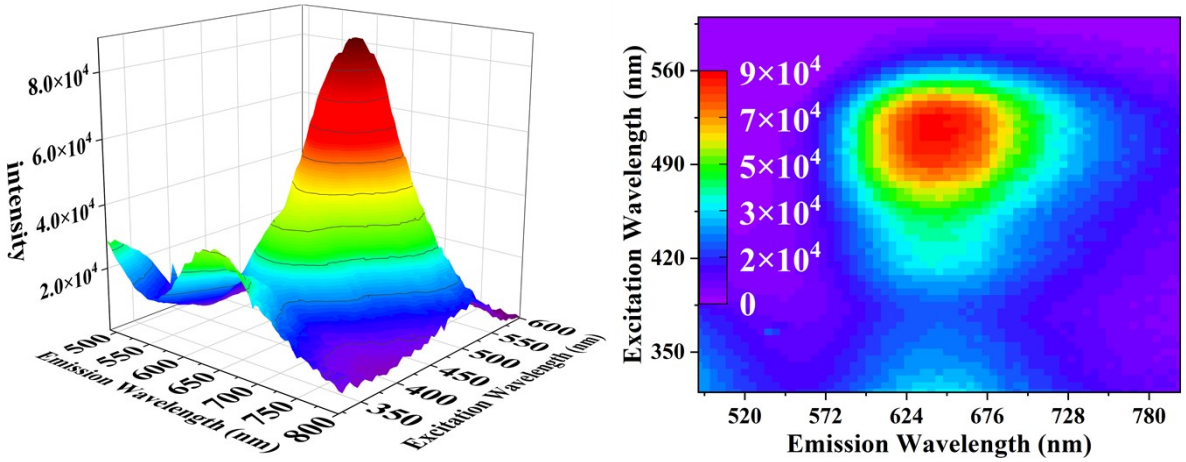

Figure S16. Excitation-dependent emission spectra in 2 wt.% PMMA film of **2** (Left: 3D Stereoscopic View, Right: 2D Planar View).

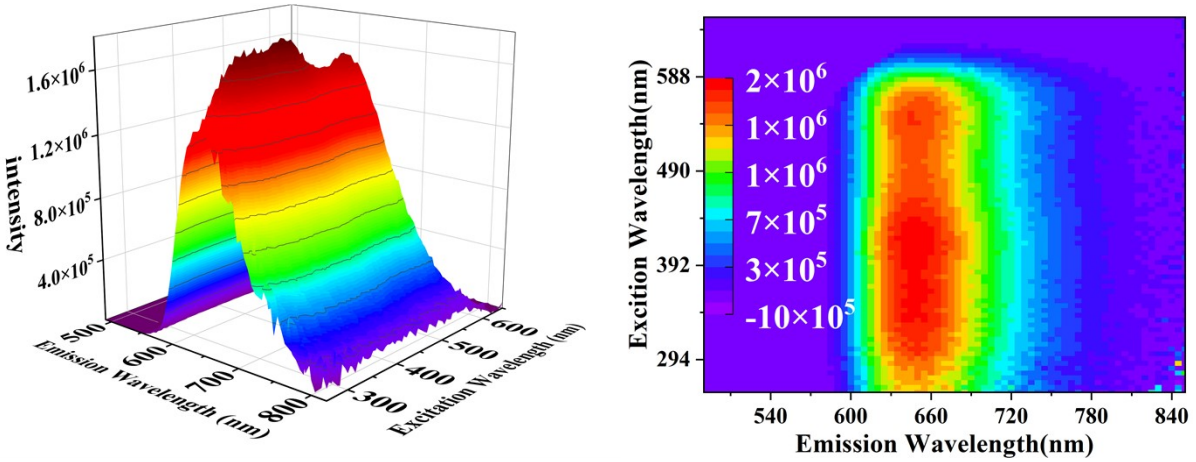

Figure S17. Excitation-dependent emission spectra of **2** in crystalline state at room temperature (Left: 3D

Stereoscopic View, Right: 2D Planar View).

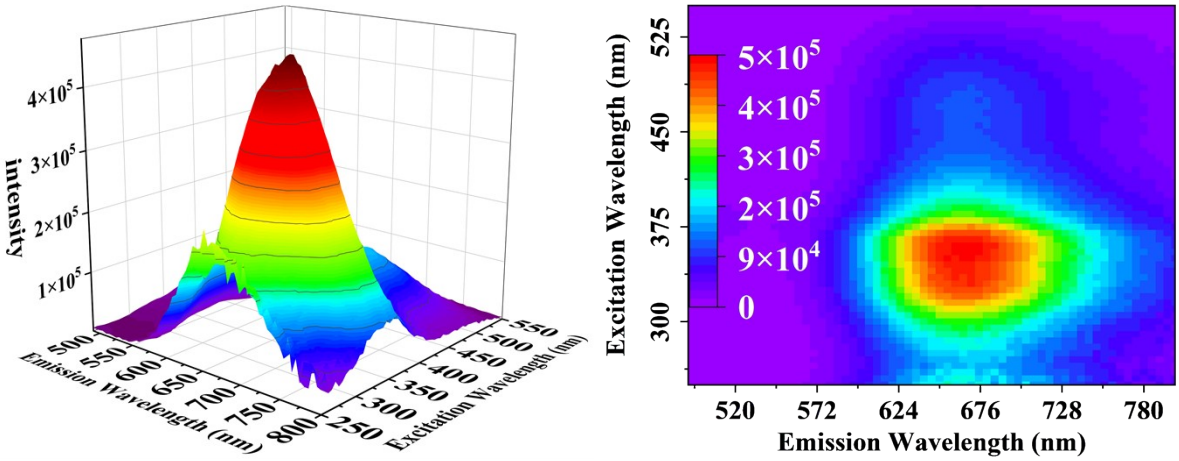

Figure S18. Excitation-dependent emission spectra of **2** in air free CH_2Cl_2 at room temperature (Left: 3D Stereoscopic View, Right: 2D Planar View).

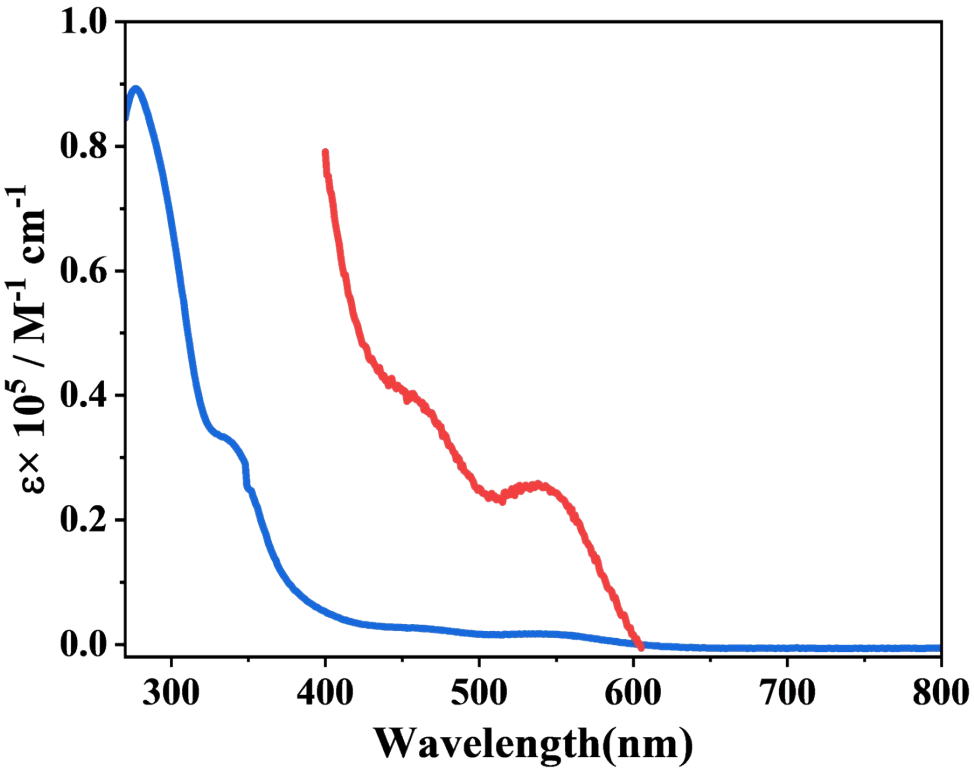

Figure S19. UV–Vis absorption spectra of **d** (blue) in CH_2Cl_2 at room temperature, for clarity, the red line is obtained by enlarging the data of the blue line by 15 times.

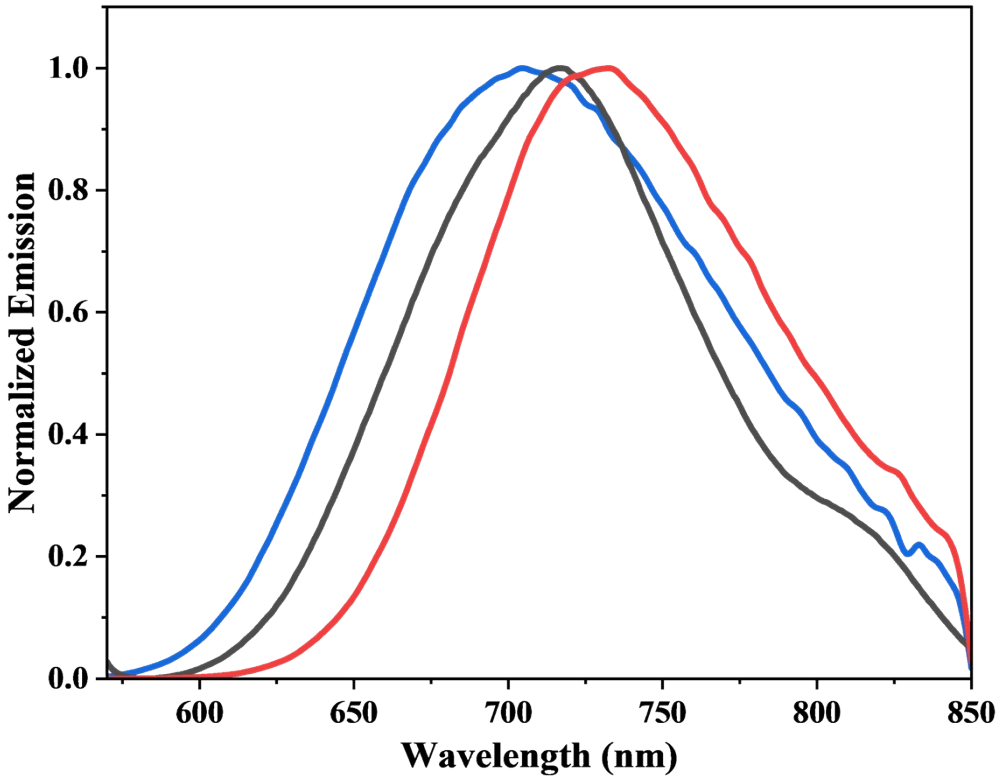

Figure S20. Normalized emission spectra of complex **d** in 2 wt.% PMMA film (blue), 10^{-5} mol/L CH_2Cl_2 solution (black), and crystalline state (red).

Table S1. The Photoluminescence data of complexes **1** and **2** doped in TCTA and 26DCzPPy[a].

Complex	Medium (298K)		Emission (λ_{max}/ nm)	τ (μs)
1	TCTA	1 wt.%	637	3.57
		2 wt.%	642	4.33
		4 wt.%	644	0.77
		6 wt.%	647	1.31
		10 wt.%	649	0.35
		20 wt.%	650	2.90
2	TCTA	1 wt.%	633	2.70
		2 wt.%	635	3.54
		4 wt.%	640	2.01
		6 wt.%	641	28.40
		10 wt.%	646	3.86
		20 wt.%	648	12.67
1	26DCzPPy	1 wt.%	635	3.76
		2 wt.%	636	2.95
		4 wt.%	637	4.73

		6 wt.%	640	3.74
		10 wt.%	643	3.79
		20 wt.%	645	3.63
2	26DCzPPy	1 wt.%	633	5.68
		2 wt.%	635	3.32
		4 wt.%	637	2.04
		6 wt.%	643	1.86
		10 wt.%	645	3.17
		20 wt.%	647	0.81

[a] Measured at room temperature, all excitation wavelengths for emission spectra are selected as 470nm (maximum UV/visible absorption wavelength)

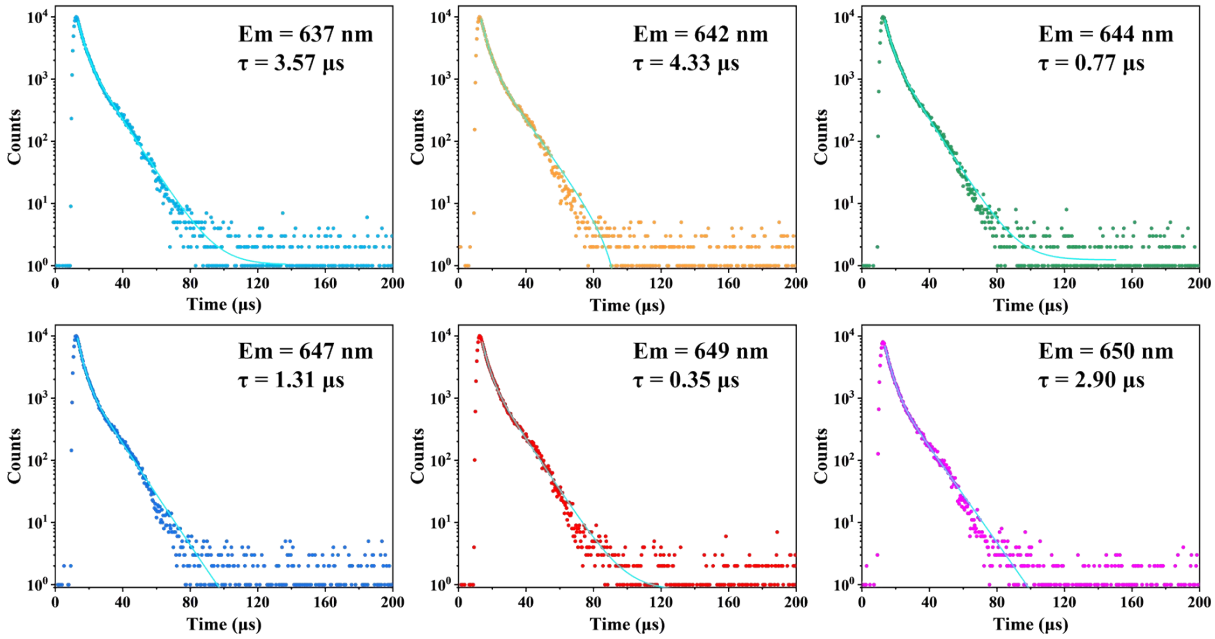

Figure S21. PL decay curves of complex **1** doping in TCTA (The concentrations from left to right and top to bottom are: 1 wt%, 2 wt%, 4 wt%, 6 wt%, 10 wt%, 20 wt%.).

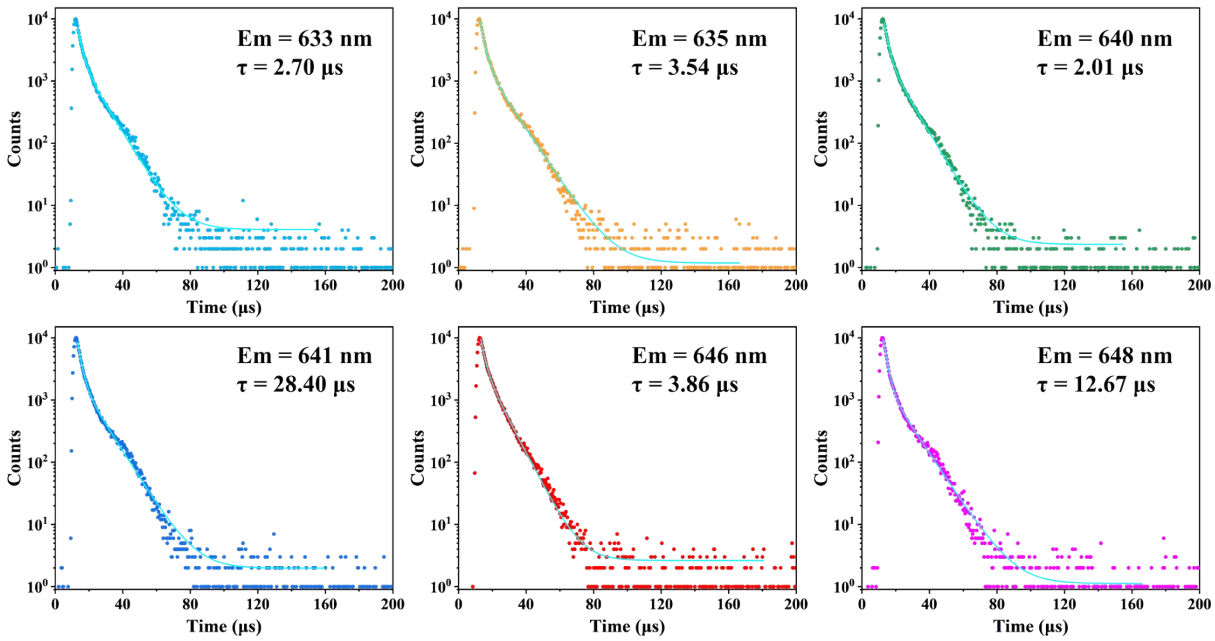

Figure S22. PL decay curves of complex **2** doping in TCTA (The concentrations from left to right and top to bottom are: 1 wt%, 2 wt%, 4 wt%, 6 wt%, 10 wt%, 20 wt%.).

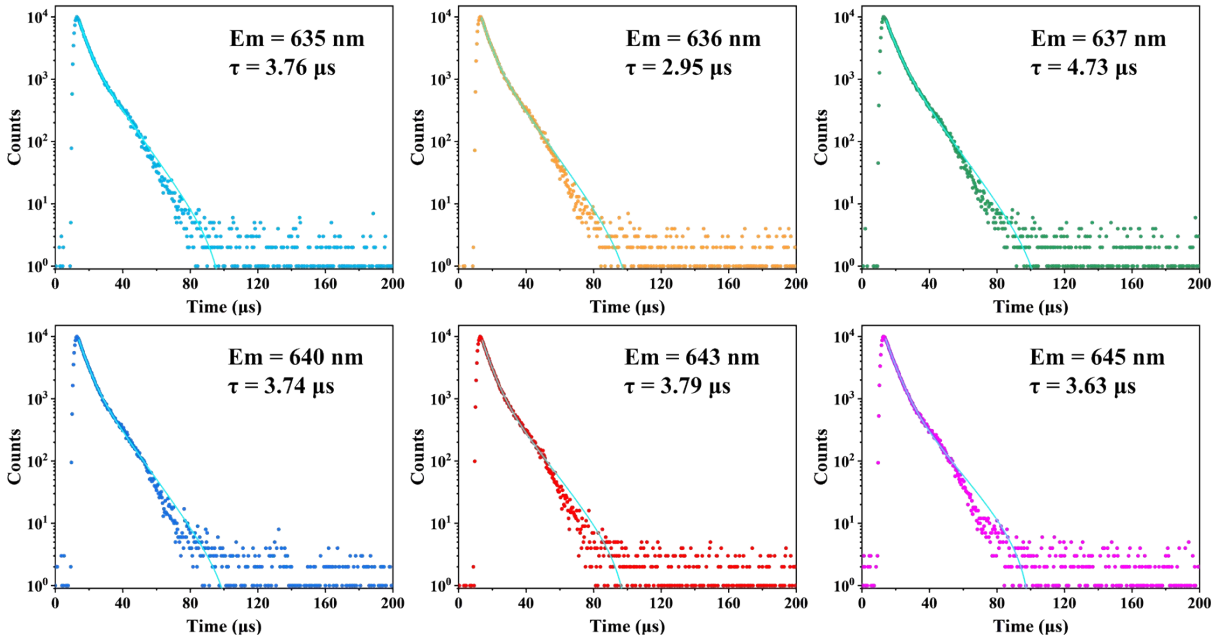

Figure S23. PL decay curves of complex **1** doping in 26DCzPPy (The concentrations from left to right and top to bottom are: 1 wt%, 2 wt%, 4 wt%, 6 wt%, 10 wt%, 20 wt%.).

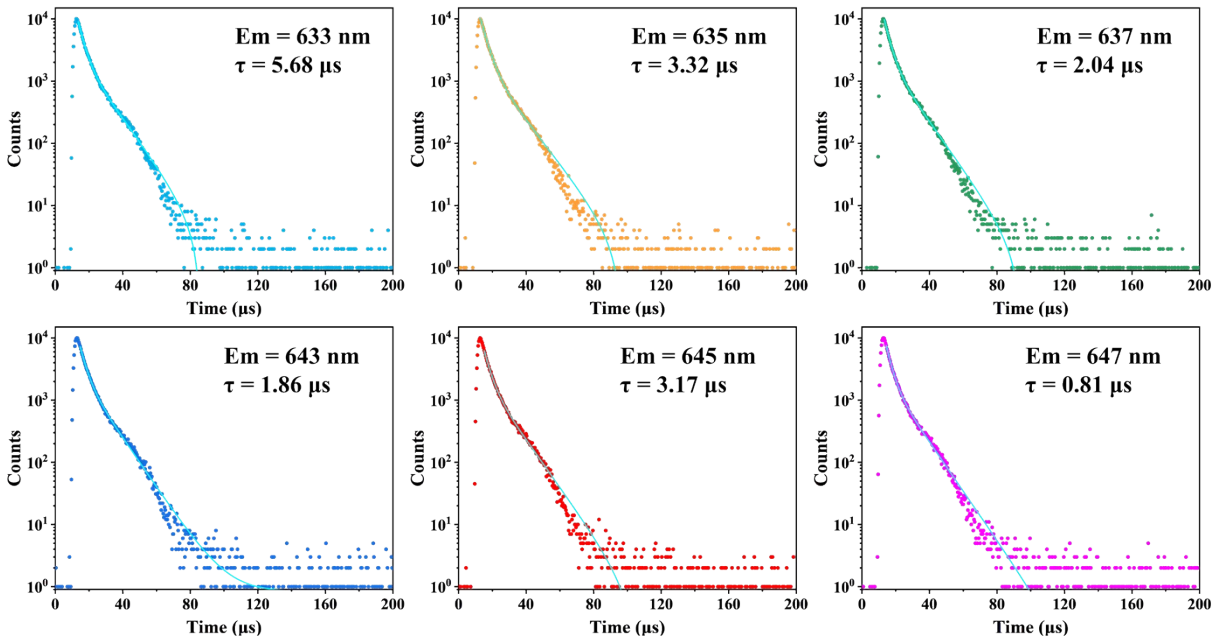

Figure S24. PL decay curves of complex **2** doping in 26DCzPPy (The concentrations from left to right and top to bottom are: 1 wt%, 2 wt%, 4 wt%, 6 wt%, 10 wt%, 20 wt%.).

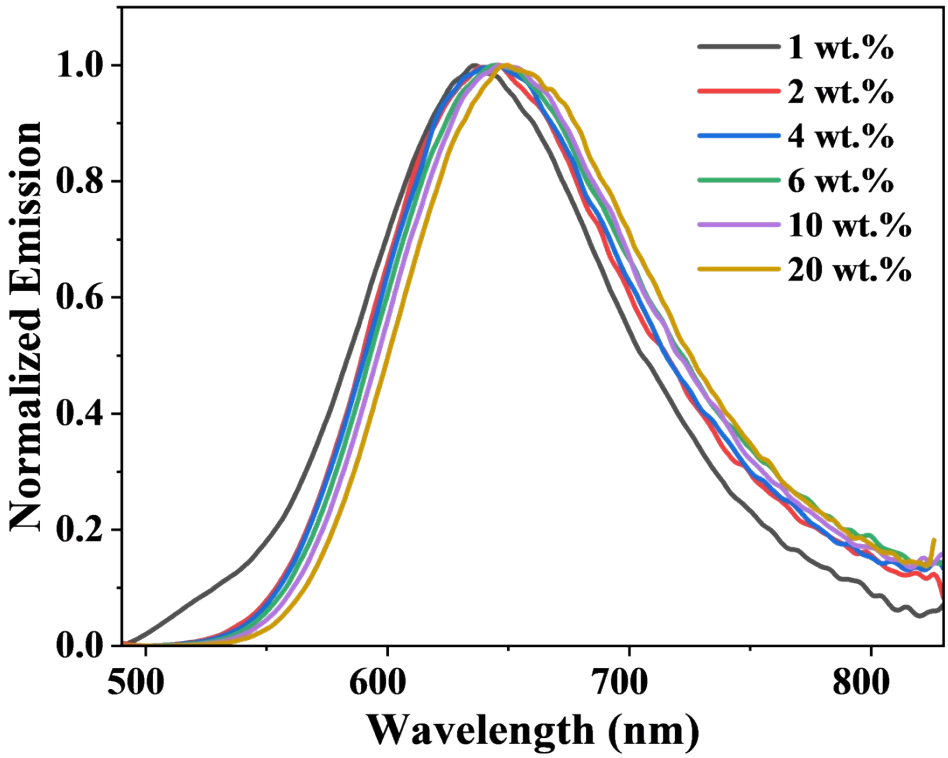

Figure S25. Normalized emission spectra in different concentrations TCTA film of complex **1**.

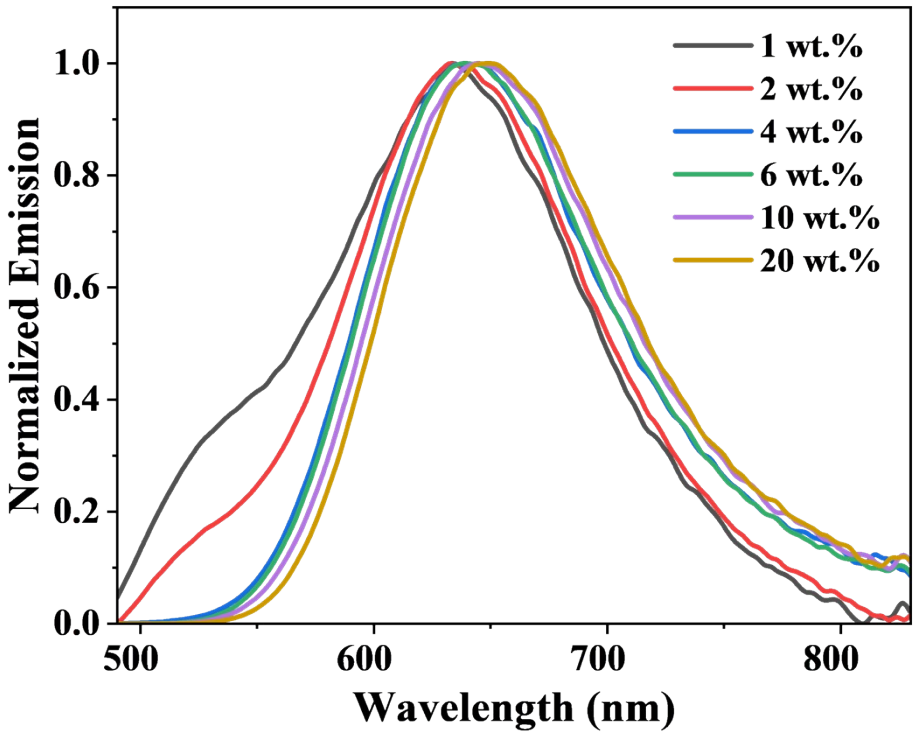

Figure S26. Normalized emission spectra in different concentrations TCTA film of complex **2** (photoluminescence).

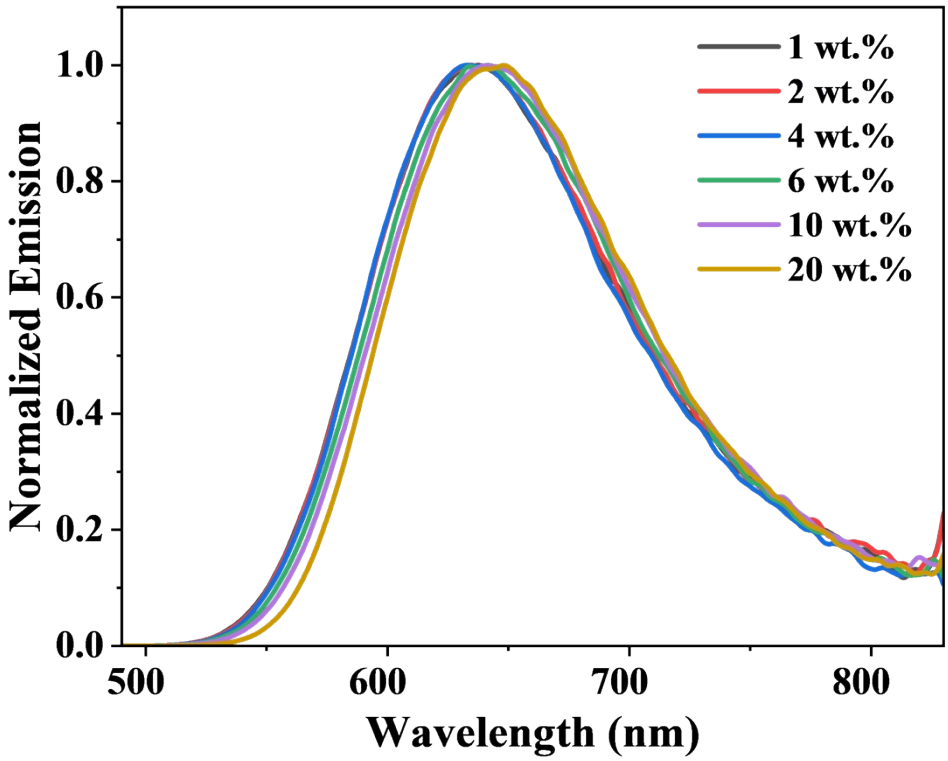

Figure S27. Normalized emission spectra in different concentrations 26DCzPPy film of complex **1** (photoluminescence).

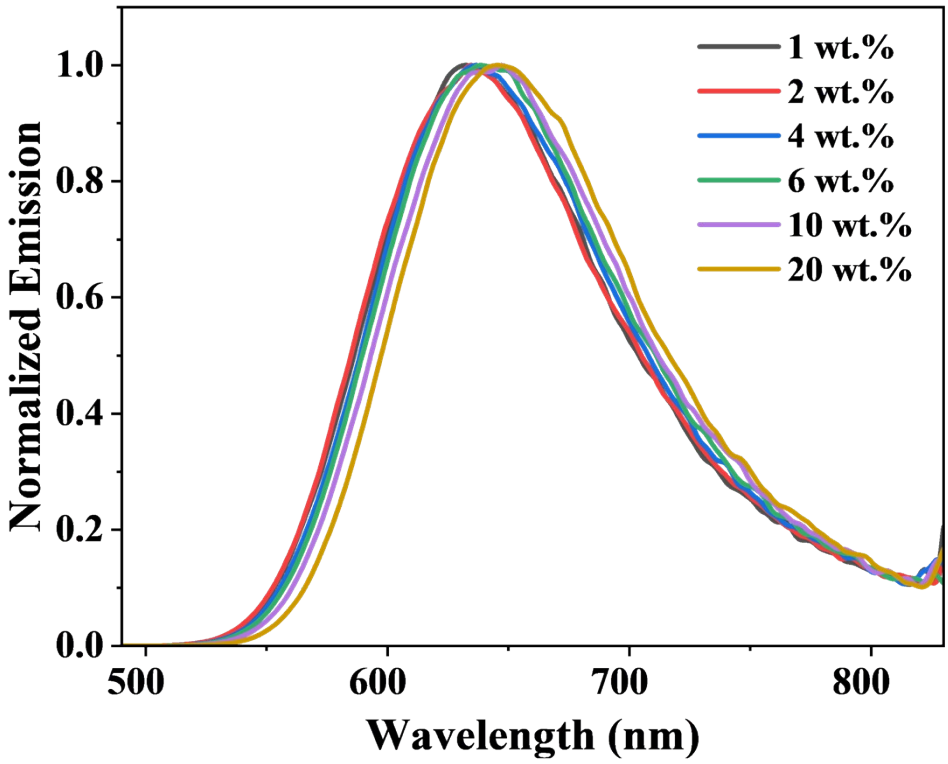

Figure S28. Normalized emission spectra in different concentrations 26DCzPPy film of complex **2** (photoluminescence).

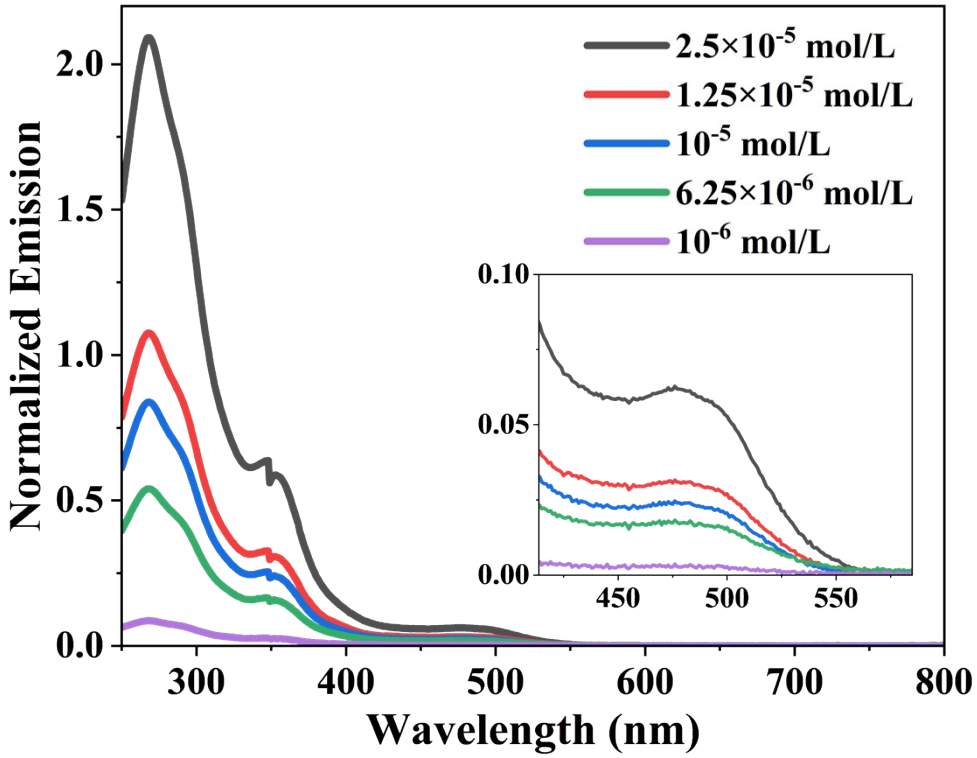

Figure S29. The UV/visible absorption spectra of complex **1** in CH_2Cl_2 at different concentrations.

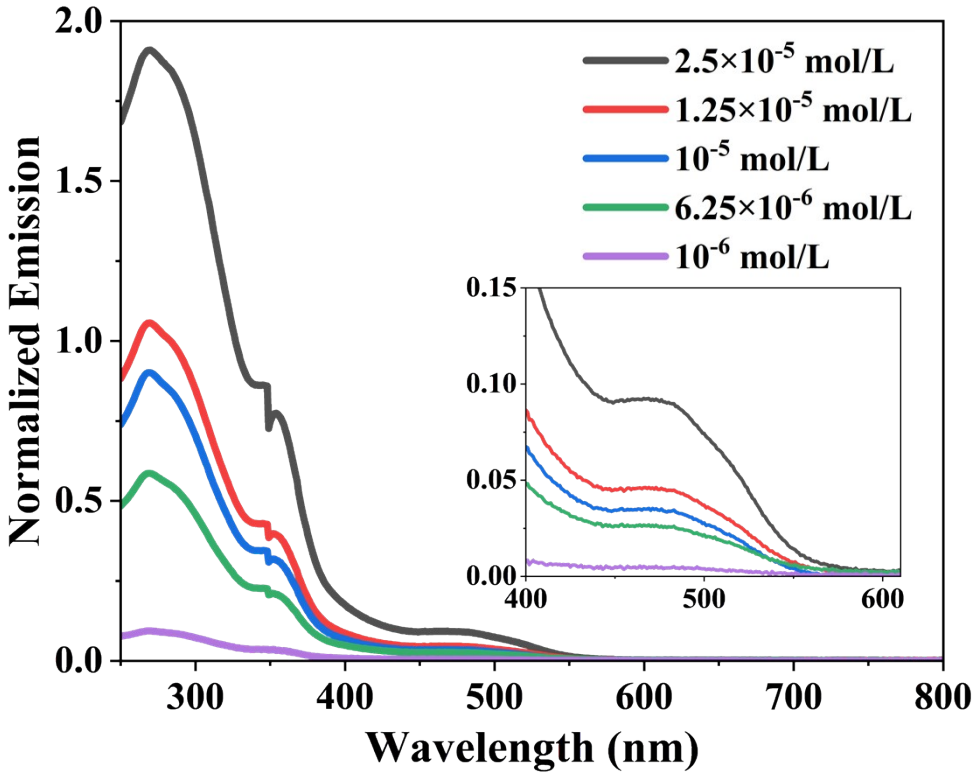

Figure S30. The UV/visible absorption spectra of complex **2** in CH_2Cl_2 at different concentrations.

5. Thermogravimetric analysis (TGA) and Cyclic voltammetry data

The thermal stability of luminescent materials is an important indicator for the preparation of OLED devices by vapor deposition method, and materials with strong thermal stability will also be widely used in more optoelectronic fields. The complexes were subjected to thermogravimetric analysis (TGA) testing in nitrogen environment, starting from room temperature (35℃) and heating at a rate of 10℃/min to 800℃. The TGA curves of two complexes were measured.

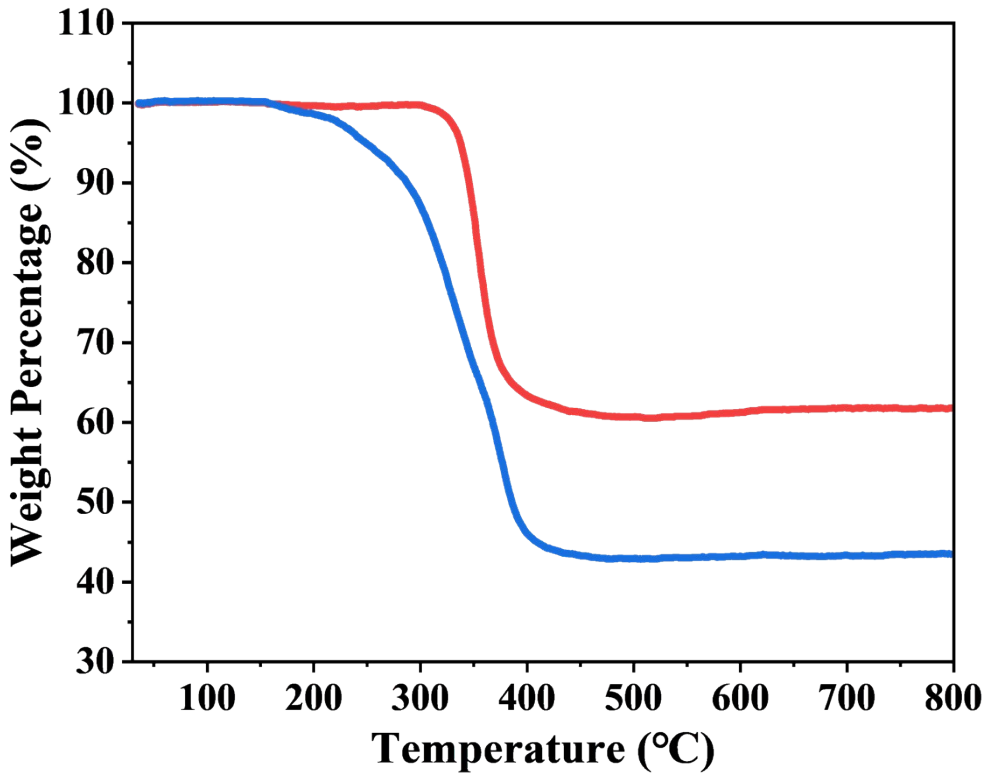

Figure S31. TGA curve of complex **1** (red) and **2** (blued).

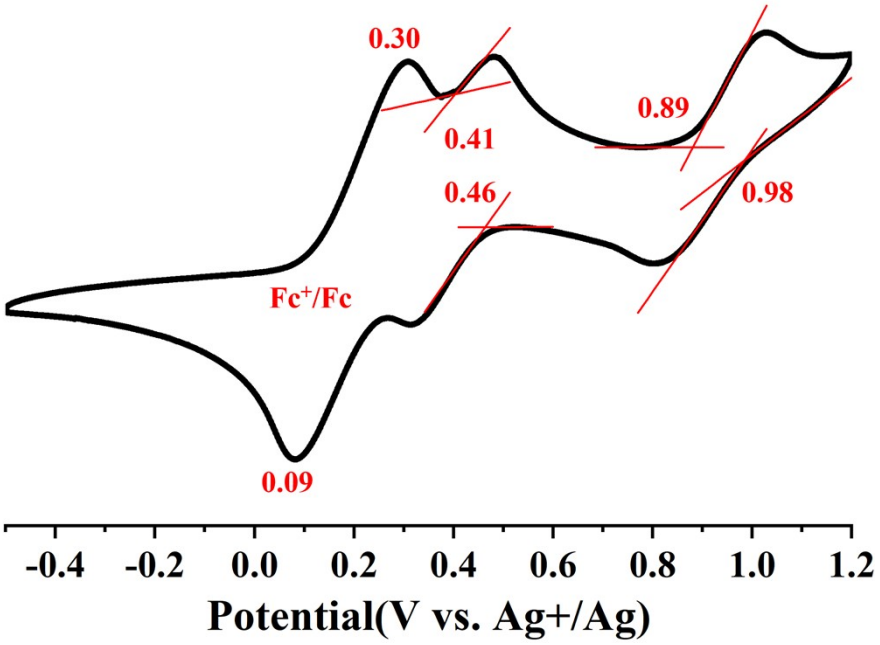

Figure S32. Cyclic voltammetry data of **1**

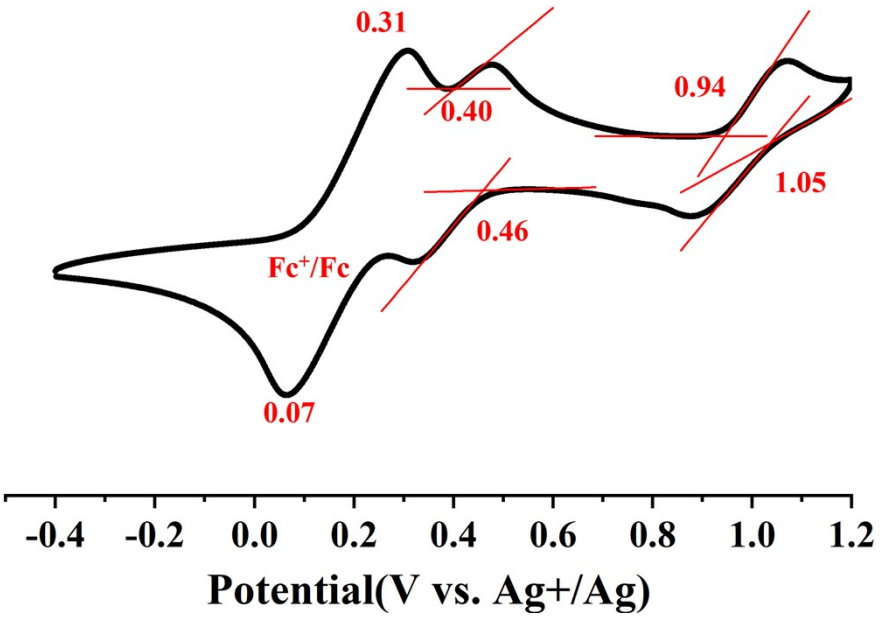

Figure S33. Cyclic voltammetry data of **2**.

6. OLED device configuration

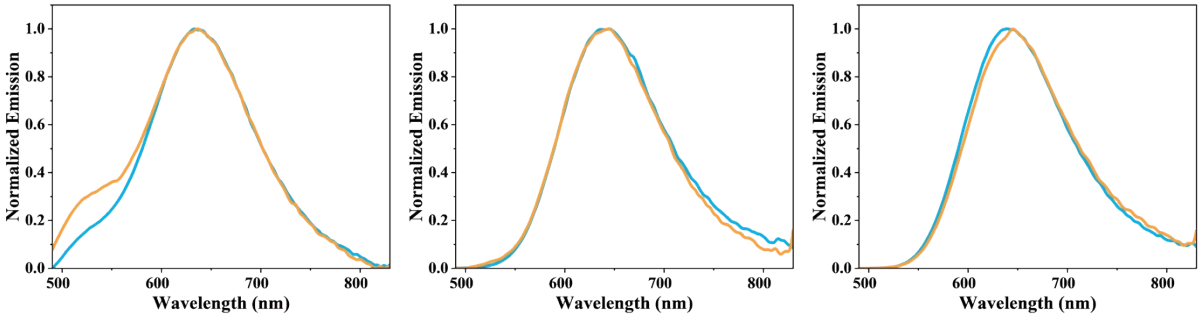

Figure S34. Complex **2** is doped into TCTA at a doping concentration of 2 wt.%, 4 wt.%, 6 wt.%, blue (r.t.), orange (heat to 170 ℃ and hold for half an hour, cool to r.t., and test).

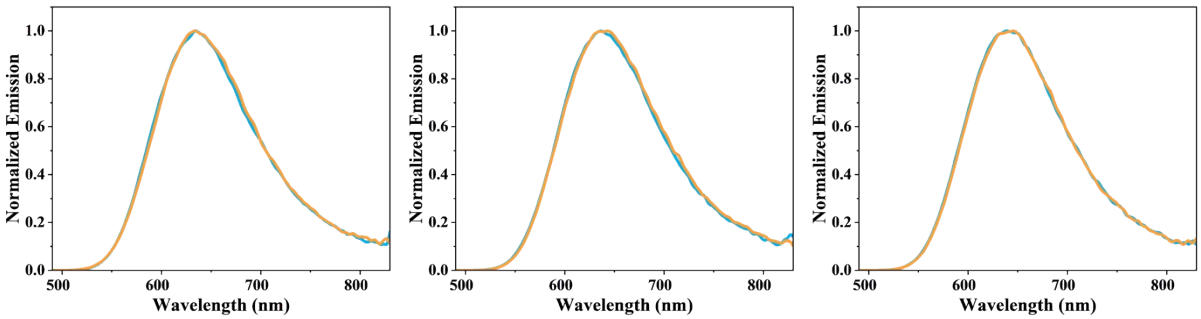

Figure S35. Complex **2** is doped into 26DCzPPy at a doping concentration of 2 wt.%, 4 wt.%, 6 wt.%, blue (r.t.), orange (heat to 170 ℃ and hold for half an hour, cool to r.t., and test).

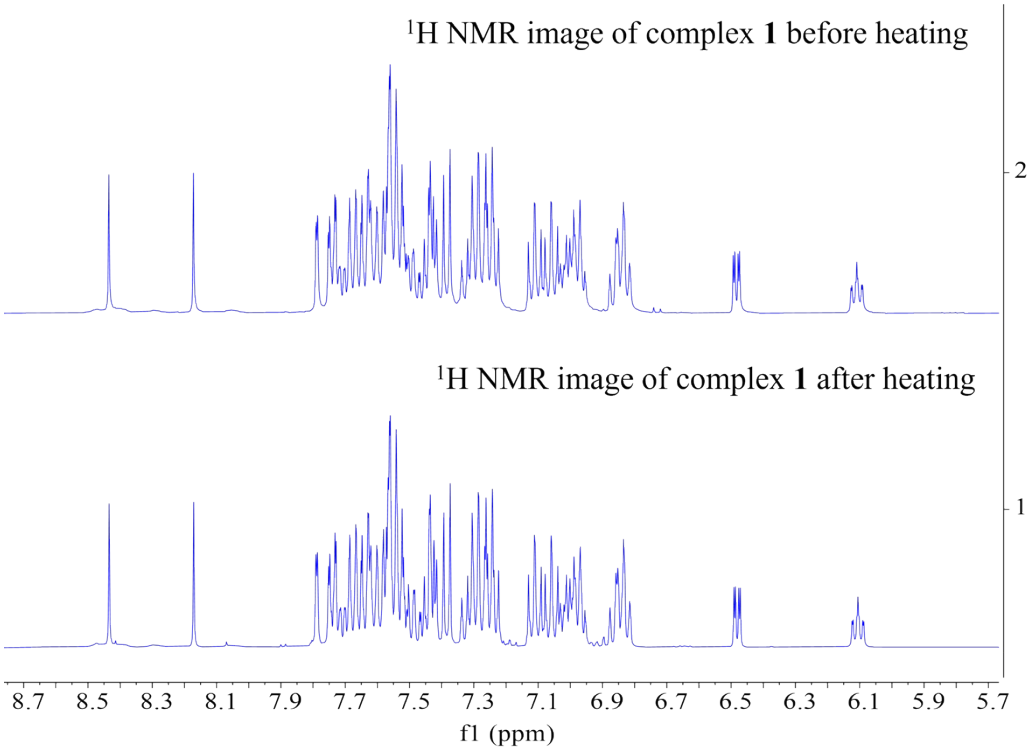

Figure S36. ^{1}H NMR comparison of complex **1** before and after heating (The following figure shows the measurement after heating complex **1** to 190 ℃ and maintaining it for 3 hours, while the above figure shows the measurement before heating).

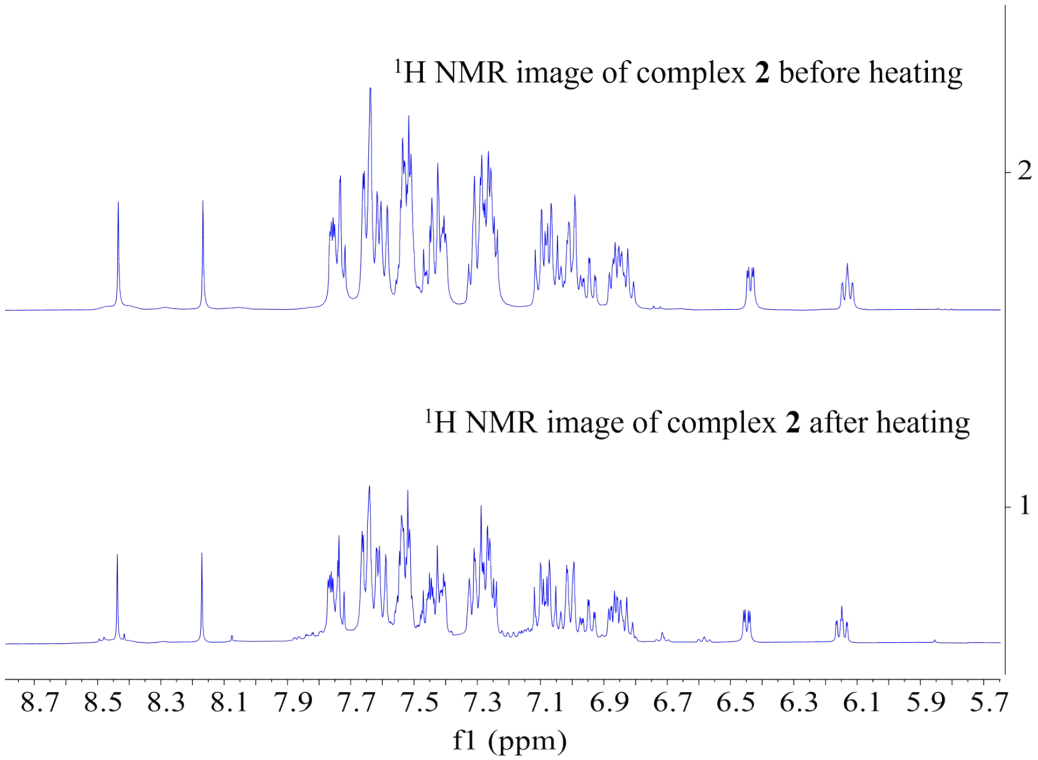

Figure S37. ¹H NMR comparison of complex **2** before and after heating (The following figure shows the measurement after heating complex **2** to 170 ℃ and maintaining it for 3 hours, while the above figure shows the measurement before heating).

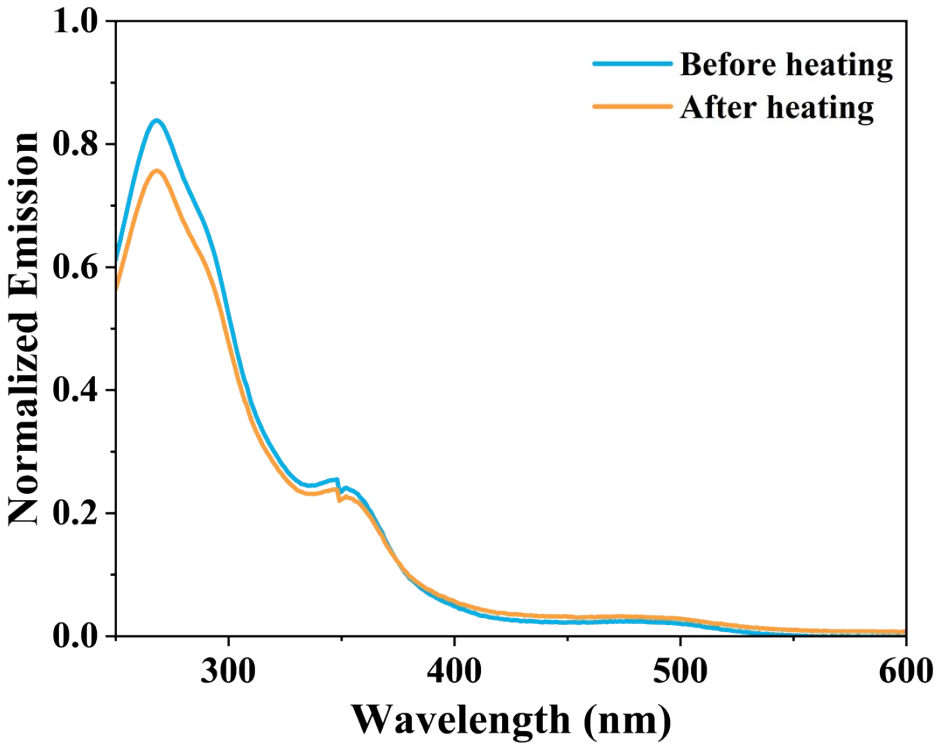

Figure S38. Comparison of UV/visible absorption spectra of complex **1** before and after heating (The orange curve represents the measurement after heating complex **1** to 190 ℃ and maintaining it for 3 h, while the blue curve represents the measurement before heating.).

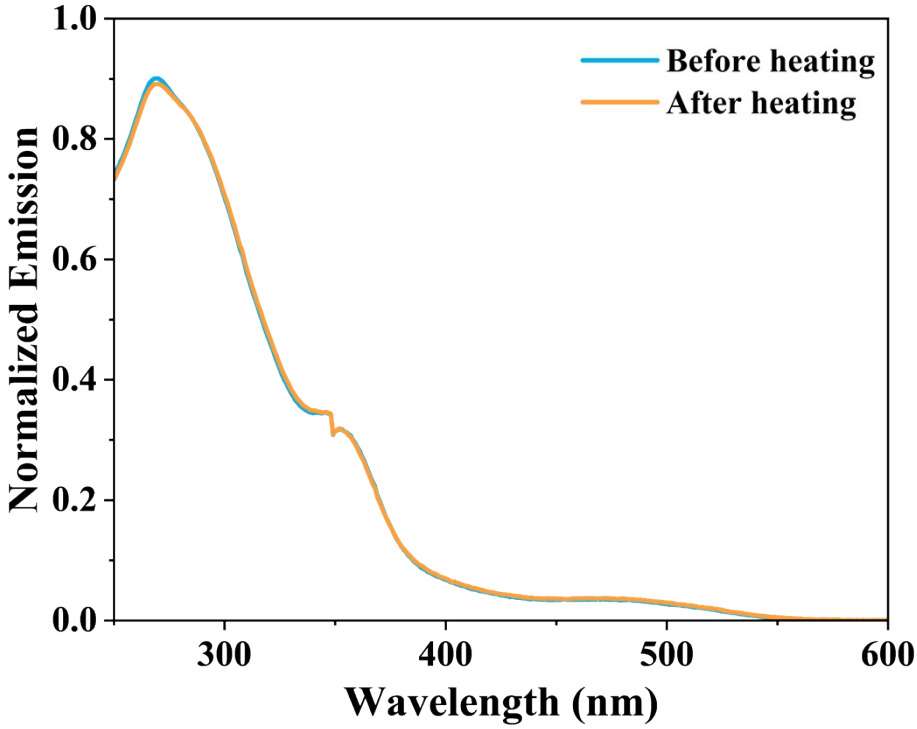

Figure S39. Comparison of UV/visible absorption spectra of complex **2** before and after heating (The orange curve represents the measurement after heating complex **2** to 170 ℃ and maintaining it for 3 h, while the blue curve represents the measurement before heating.).

Figure S40. OLED devices using complex **1**.

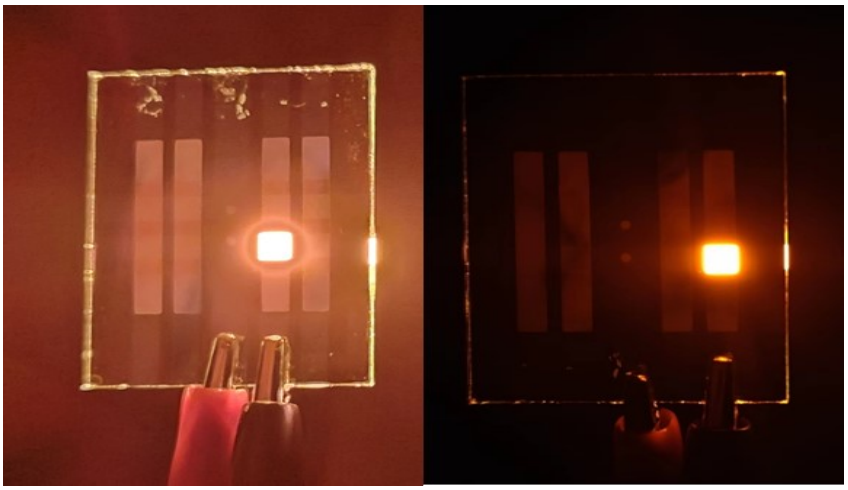

Figure S41. OLED devices using complex **2**.

7. Crystal data

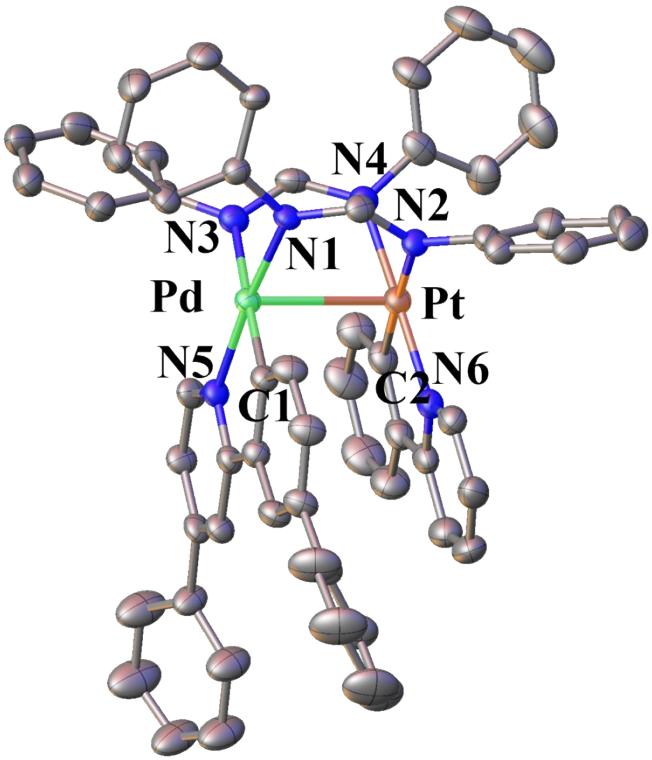

Figure S42. Crystal structure of the **1**. Hydrogen atoms are omitted.

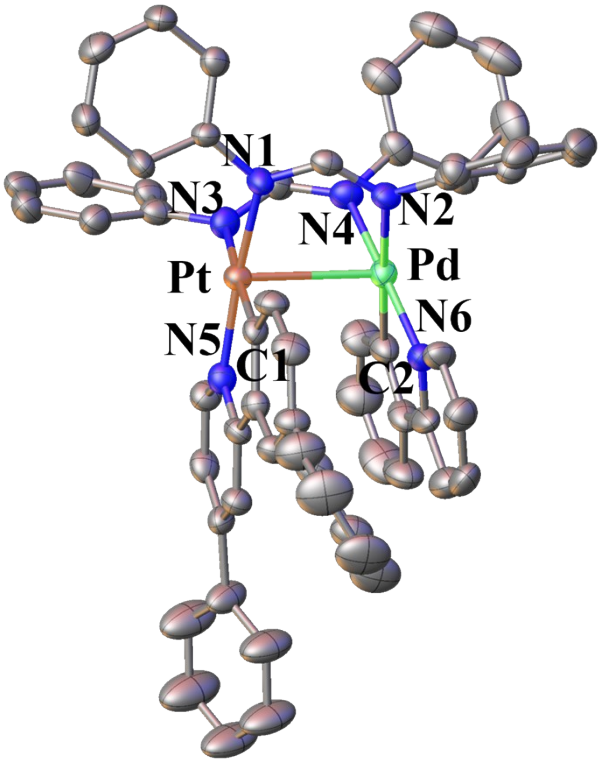

Figure S43. Crystal structure of the **2**. Hydrogen atoms are omitted.

Table S2. Summary of the crystal data of **1** and **2**.

	1	**2**
CCDC number	2311651	2311650
Empirical formula	$C_{62}H_{50}Cl_4N_6PdPt$	$C_{62}H_{50}Cl_4N_6PdPt$
Formula weight	1322.37	1322.37
Temperature/K	213.0 K	213.0 K
Crystal system	orthorhombic	orthorhombic
Space group	Pbca	Pbca
a/Å	23.5541(6)	23.6443(6)
b/Å	16.6473(4)	16.6182(4)
c/Å	28.8957(7)	28.8904(7)
α/°	90	90
β/°	90	90
γ/°	90	90
Volume/Å^3	11330.4(5)	11351.8(5)
z	8	8
ρ_{calc}mg/cm^3	1.550	1.547
μ/mm^{-1}	6.252	6.240
F(000)	5248.0	5248.0
Crystal size/mm^3	0.07 × 0.07 × 0.05	0.07 × 0.07 × 0.05
2Θ range for data collection	7.768 to 109.992	7.768 to 110.226
Index ranges	-28 ≤ h ≤ 28, -18 ≤ k ≤ 20, -33 ≤ l ≤ 35	-28 ≤ h ≤ 20, -15 ≤ k ≤ 20, -35 ≤ l ≤ 26
Reflections collected	114253	69619
Independent reflections	10778 [$R_{(int)}$ =0.0928, R_{sigma} =0.0464]	10818 [$R_{(int)}$ =0.0878, R_{sigma} =0.0836]
Data/restraints/parameters	10778/36/640	10818/37/601
Goodness-of-fit on F^2	1.049	1.075
Final R indexes [I>=2σ (I)]	R_1 = 0.0517, wR_2 = 0.1390	R_1 = 0.0576, wR_2 = 0.1483
Final R indexes [all data]	R_1 = 0.0686, wR2 = 0.1491	R_1 = 0.1106, wR2 = 0.1669
Largest diff. peak/hole / e Å^{-3}	1.02/-1.42	0.89/-1.17

Table S3. Bond lengths [Å] and angles [°] for **1**.

Bond lengths [Å]			
Pd-N1	2.044(4)	Pt-N4	2.031(5)
Pd-N3	2.140(5)	Pt-N2	2.144(5)
Pd-N5	2.037(4)	Pt-N6	2.023(5)
Pd-C1	1.980(6)	Pt-C2	2.004(6)
Pd-Pt	2.8557(5)		

Bond angles [°]			
N3-Pd-N1	88.73(19)	N2-Pt-N4	87.42(19)
N5-Pd-N3	97.66(18)	N6-Pt-N2	97.00(18)
C1-Pd-N5	81.3(2)	C2-Pt-N6	80.7(2)
N1-Pd-C1	92.2(2)	N4-Pt-C2	94.8(2)

Table S4. Bond lengths [Å] and angles [°] for **2**.

Bond lengths [Å]			
Pt-N1	2.034(5)	Pd-N4	2.033(6)
Pt-N3	2.118(6)	Pd-N2	2.149(5)
Pt-N5	2.034(5)	Pd-N6	2.054(6)
Pt-C1	1.963(7)	Pd-C2	1.986(8)
Pd-Pt	2.8548(6)		

Bond angles [°]			
N3-Pt-N1	87.7(2)	N2-Pd-N4	88.0(2)
N5-Pt-N3	97.7(2)	N6-Pd-N2	96.1(2)
C1-Pt-N5	81.0(3)	C2-Pd-N6	81.5(3)
N1-Pt-C1	93.4(3)	N4-Pd-C2	94.4(3)

8. NMR and ESI-Mass spectra

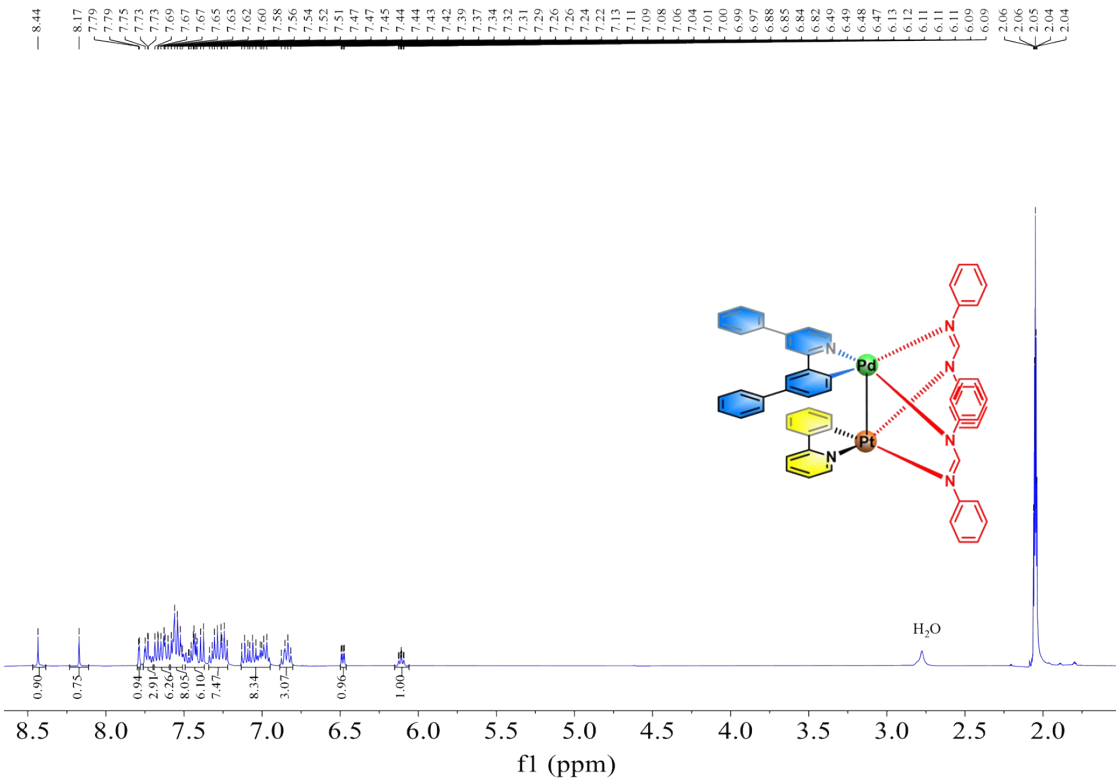

Figure S44. ^{1}H NMR spectrum of **1** in $(CD_3)_2CO$.

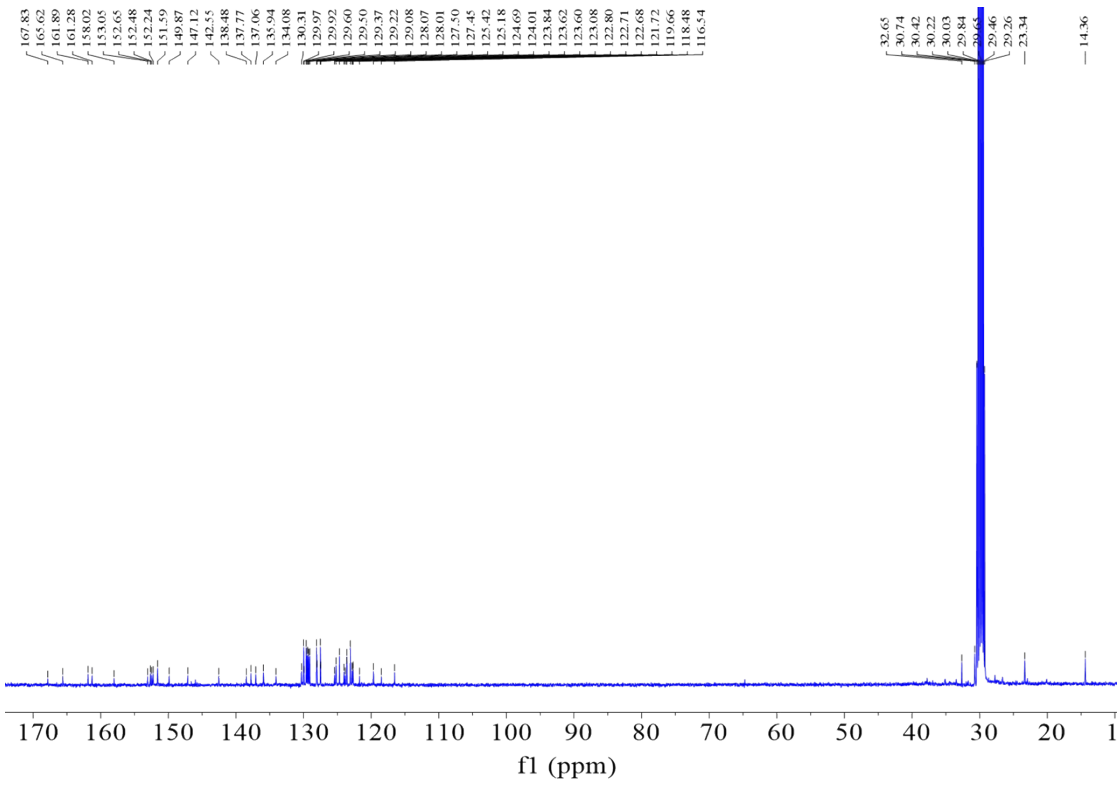

Figure S45. ^{13}C NMR spectrum of **1** in $(CD_3)_2CO$.

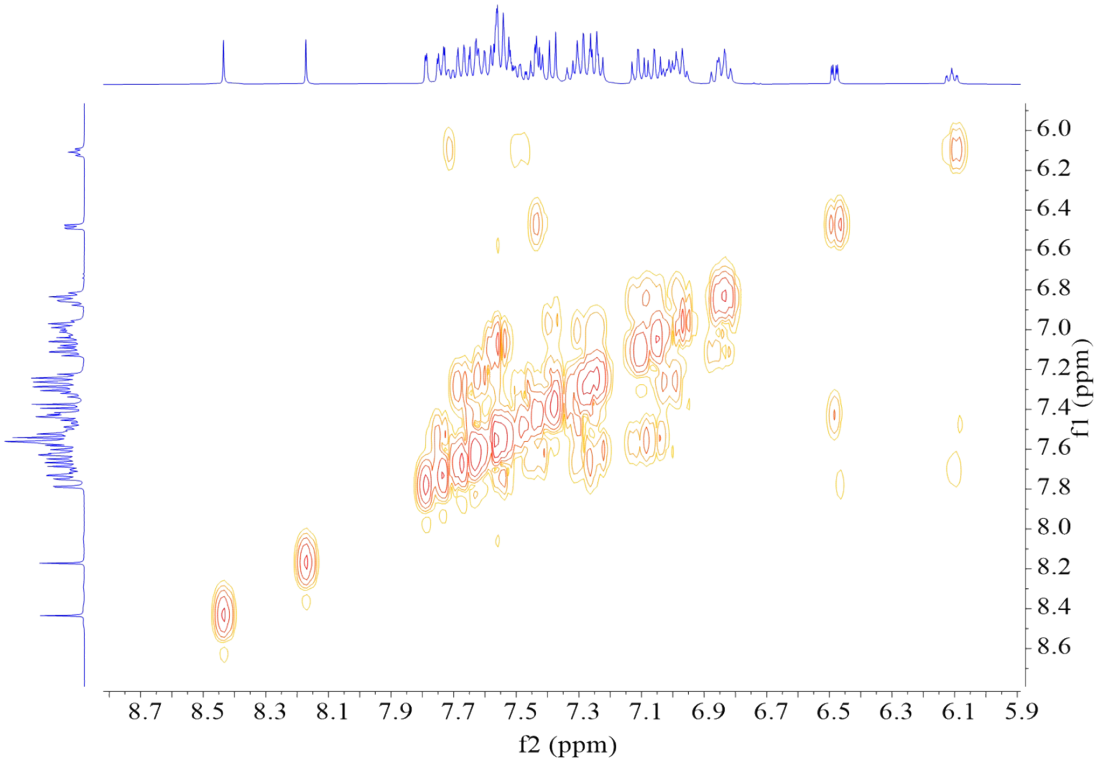

Figure S46. ^{1}H-^{1}H COSY NMR spectrum of **1** in $(CD_3)_2CO$.

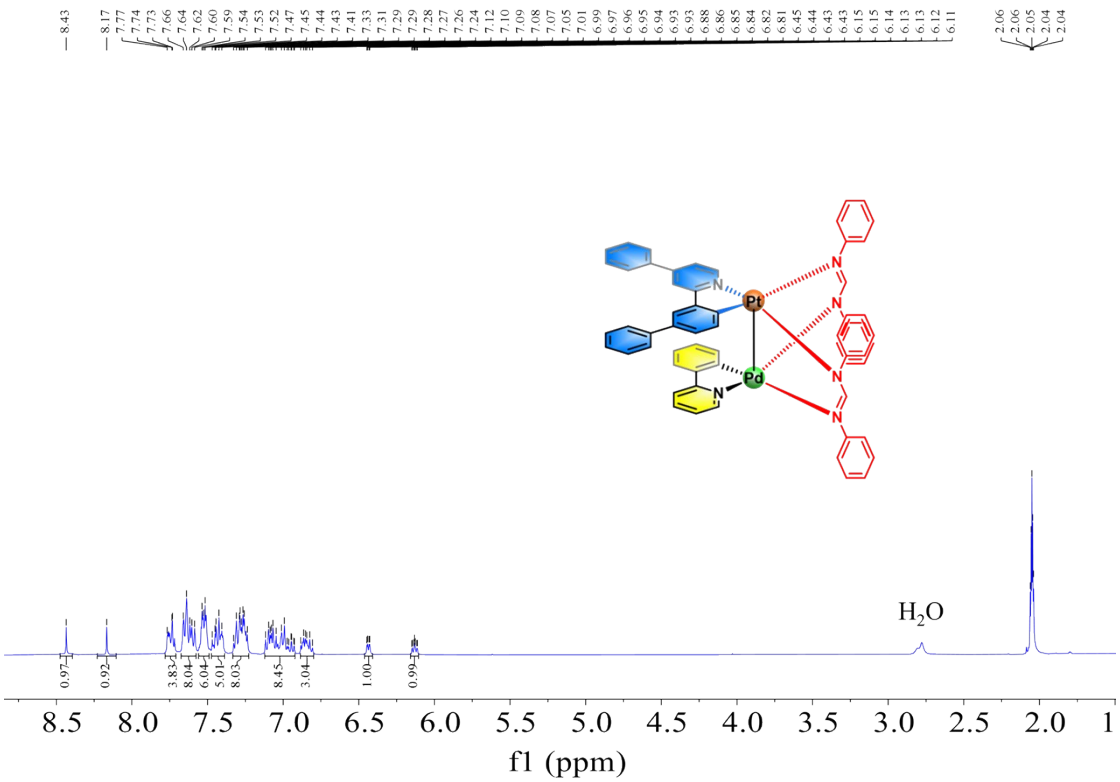

Figure S47. ^{1}H NMR spectrum of **2** in $(CD_3)_2CO$.

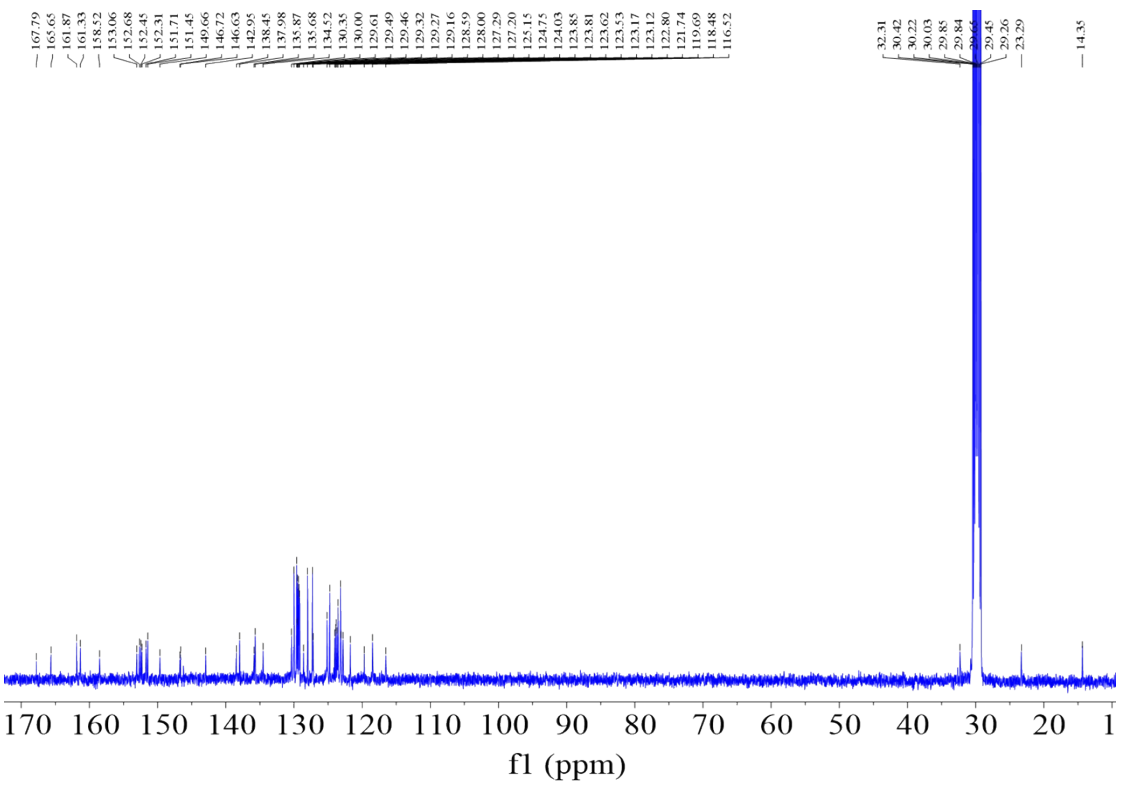

Figure S48. ^{13}C NMR spectrum of **2** in $(CD_3)_2CO$.

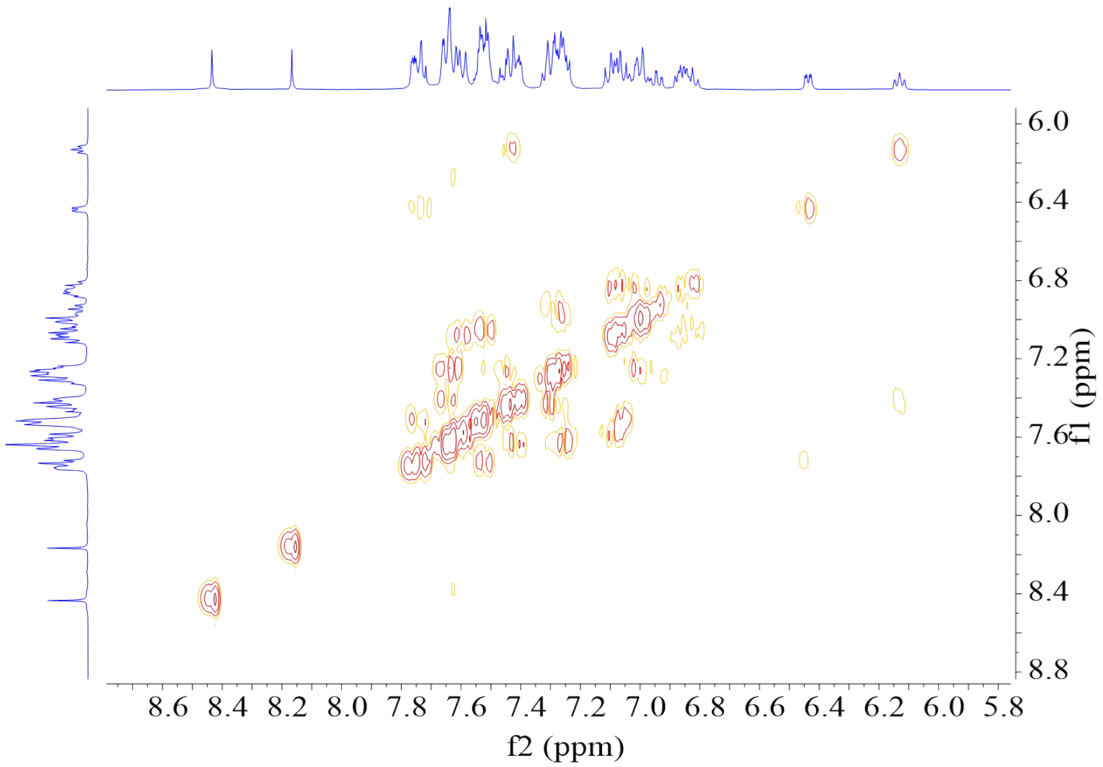

Figure S49. ^{1}H-^{1}H COSY NMR spectrum of **2** in $(CD_3)_2CO$.

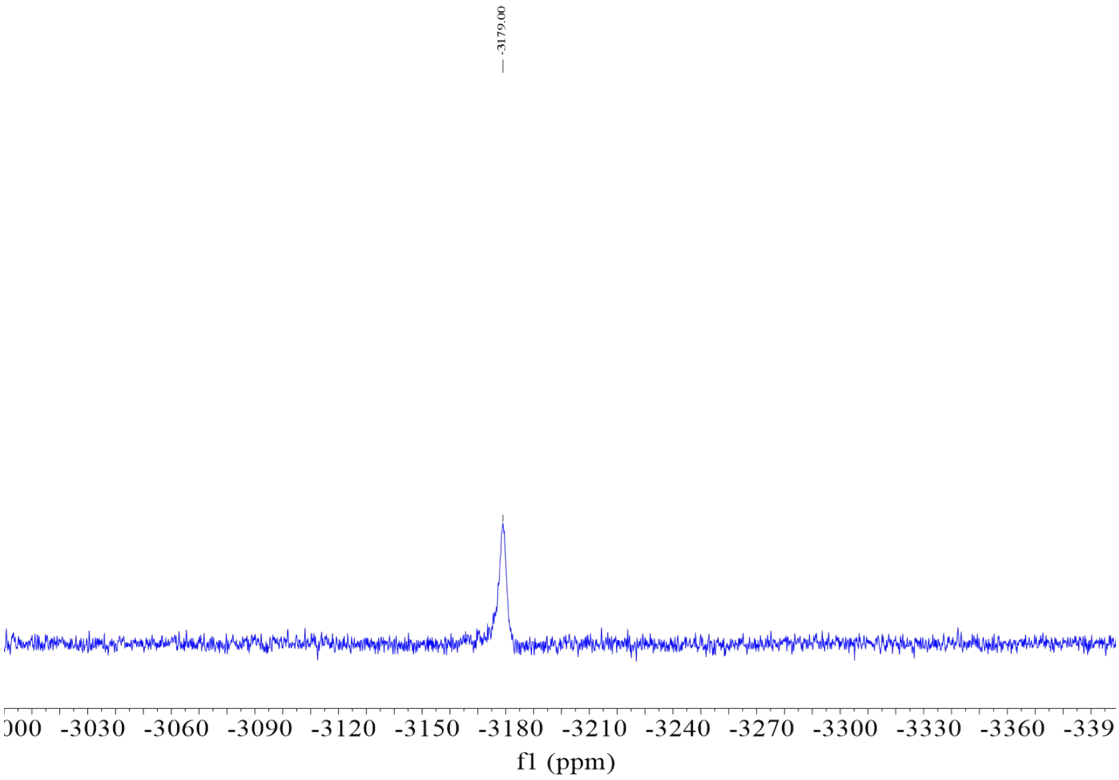

Figure S50. ^{195}Pt NMR spectrum of **1** in $CDCl_3$.

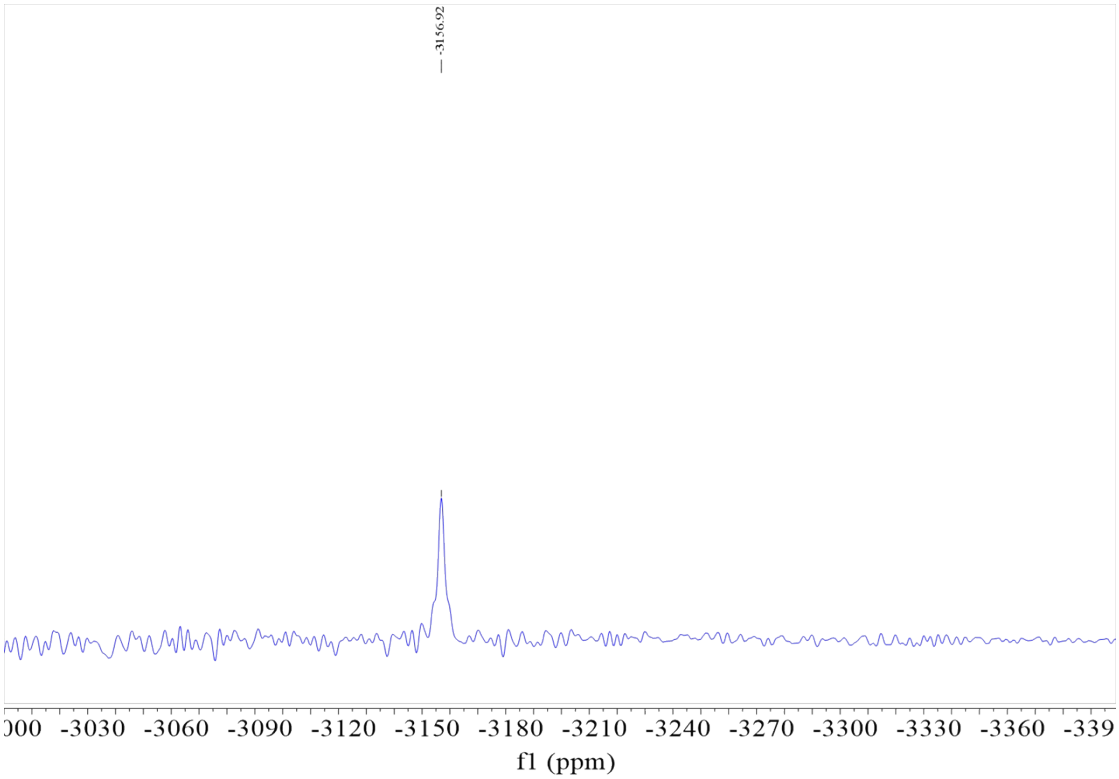

Figure S51. ^{195}Pt NMR spectrum of **2** in $CDCl_3$.

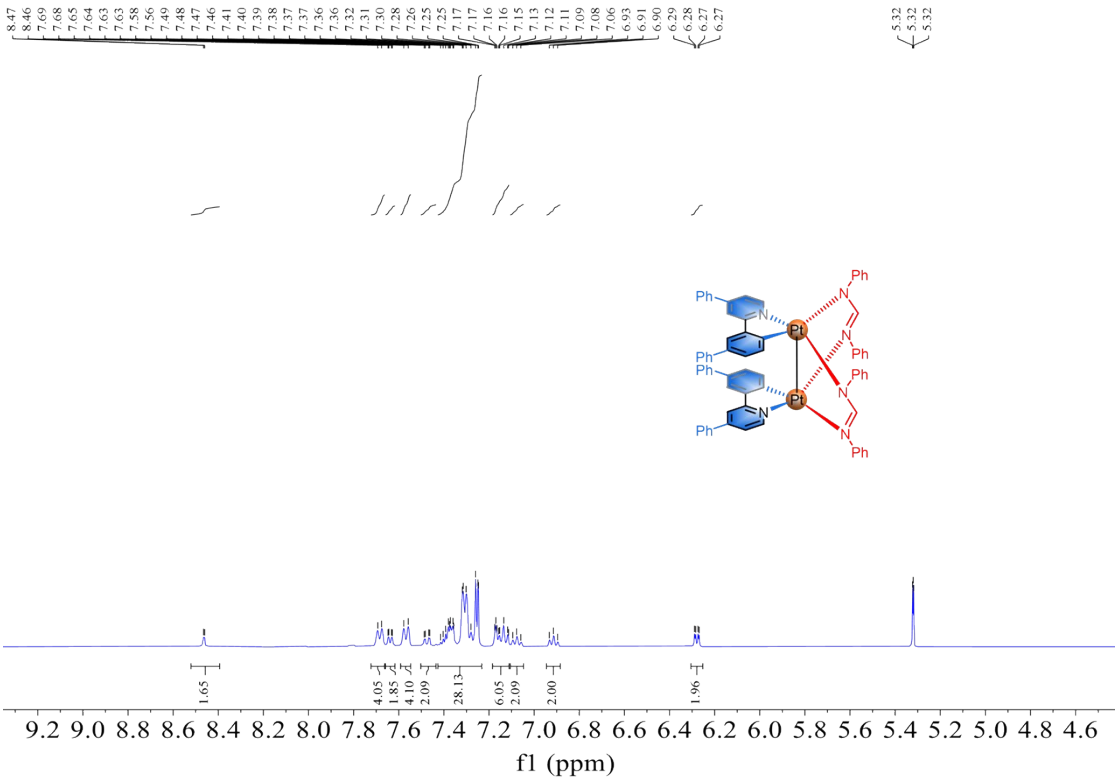

Figure S52. ^{1}H NMR spectrum of **d** in CD_2Cl_2.

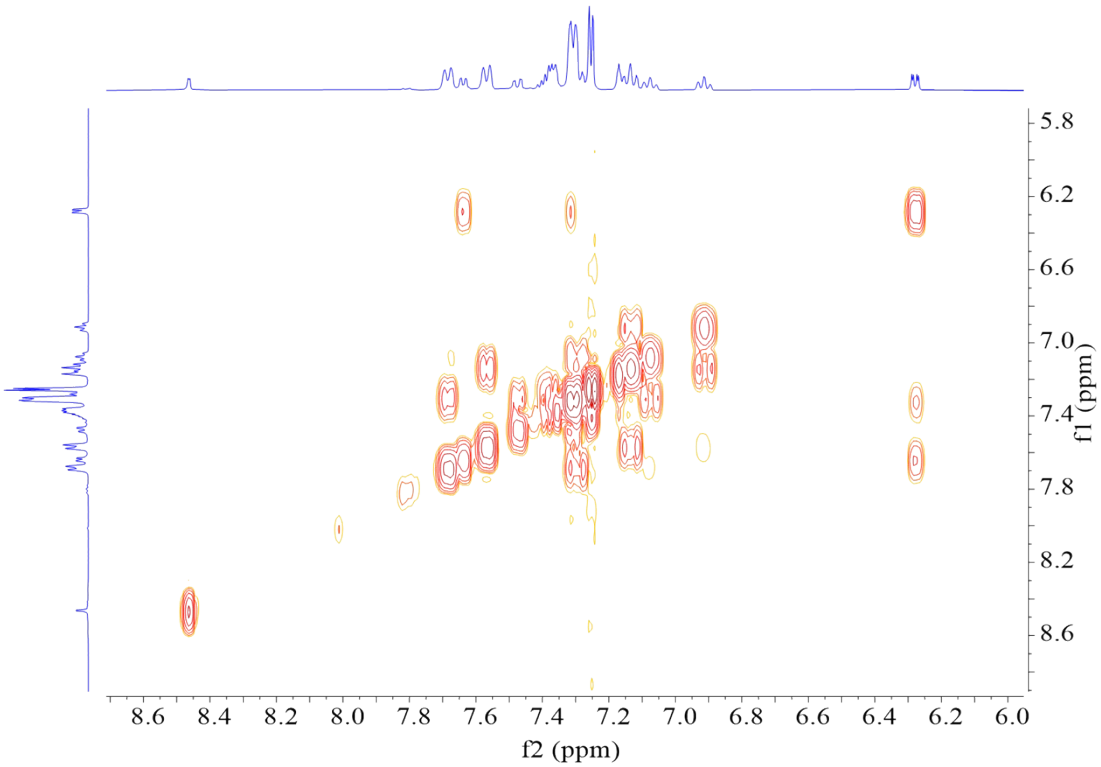

Figure S53. ^{1}H-^{1}H COSY NMR spectrum of **d** in CD_2Cl_2.

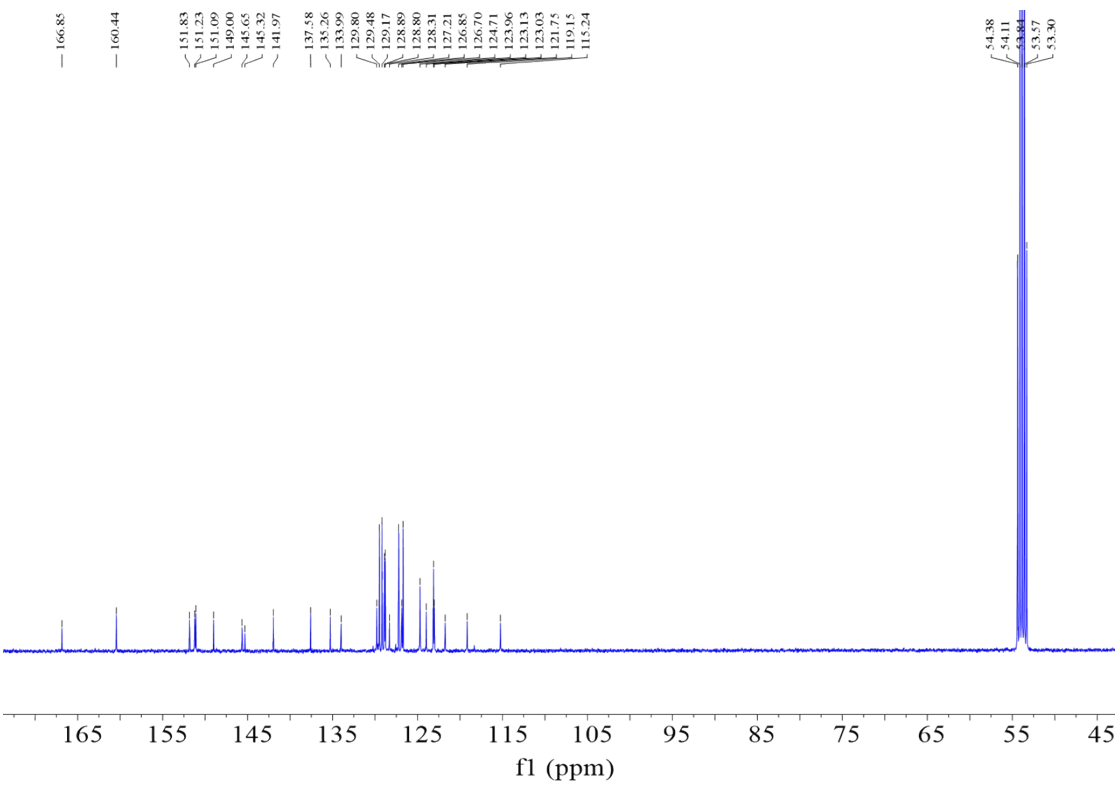

Figure S54. ^{13}C NMR spectrum of **d** in CD_2Cl_2.

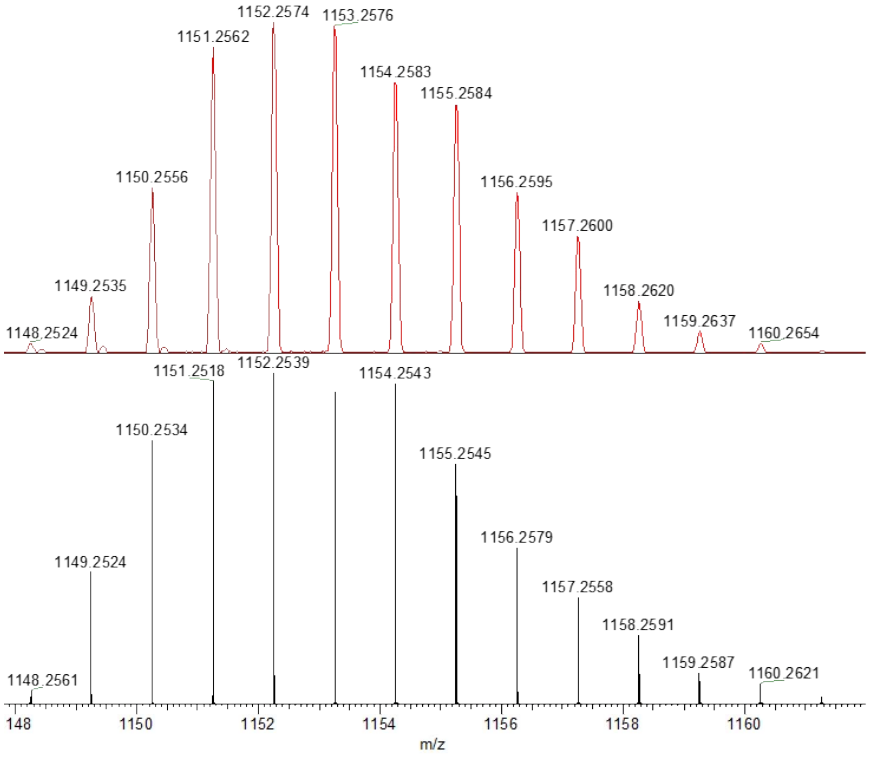

Figure S55. HR-MS spectra for **1** $[M+H]^+$.

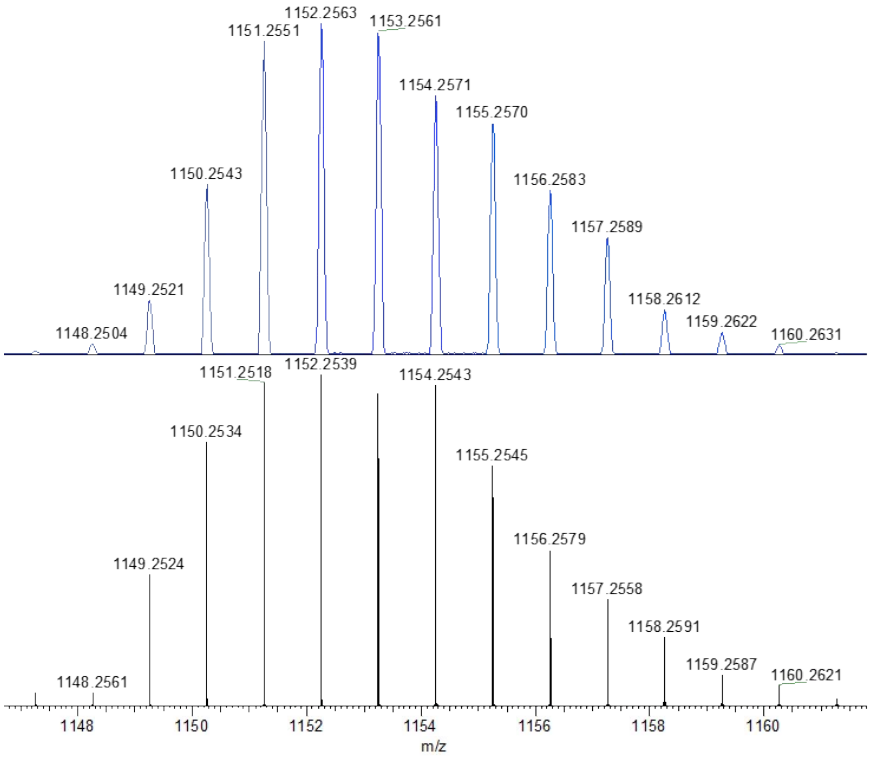

Figure S56. HR-MS spectra for **2** $[M+H]^+$.

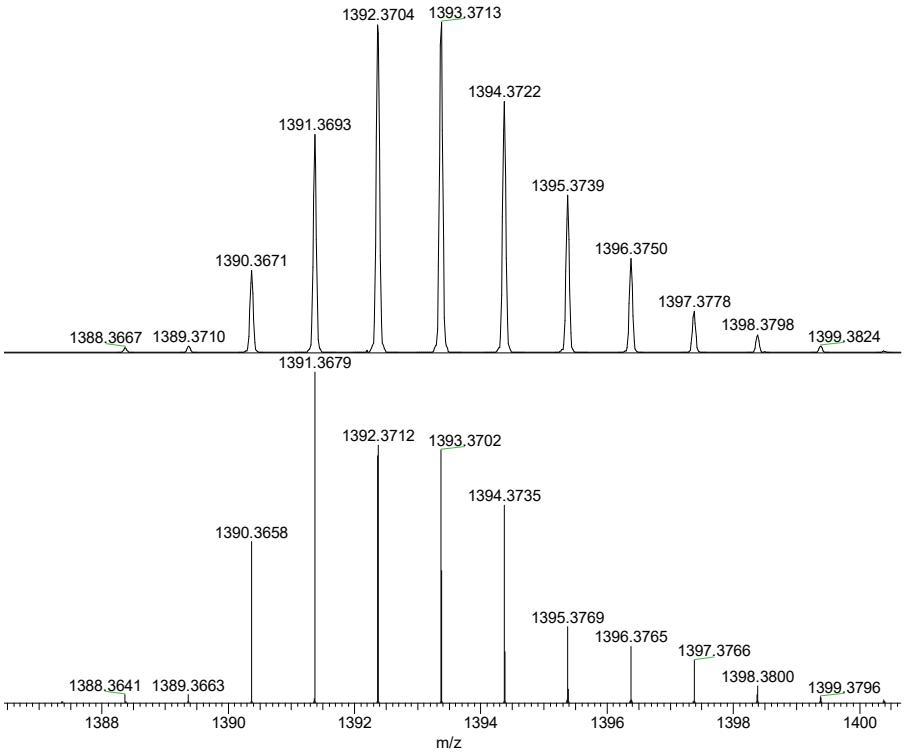

Figure S57. HR-MS spectra for **d** [M].

References

1. B. An, Z. G. Wang, L. C. Yang and X. P. Li, A Semi-Empirical Formula of the Dependence of the Fluorescence Intensity of Naphthalene on Temperature and the Oxygen Concentration, *Journal of Applied Spectroscopy*, 2017, **84**, 555-559.
2. S. Pluczyk, M. Vasylieva and P. Data, Using Cyclic Voltammetry, UV-Vis-NIR, and EPR Spectroelectrochemistry to Analyze Organic Compounds, *Journal of Visualized Experiments*, 2018, DOI: 10.3791/56656.
3. K. Wei, F. Liao, H. Huang, M. Shao, H. Lin, Y. Liu and Z. Kang, Simple Semiempirical Method for the Location Determination of HOMO and LUMO of Carbon Dots, *The Journal of Physical Chemistry C*, 2021, **125**, 7451-7457.
4. N. R. Yi Sun, Shu-Bin Zhao, Krista Huszarik, Wen-Li Jia, Rui-Yao Wang, and a. S. W. Donal Macartney, Enhancing Electron Accepting Ability of Triarylboron via π-Conjugation with 2,2'-Bipy and Metal Chelation: 5,5'-Bis(BMes2)-2,2'-bipy and Its Metal Complexes, *Journal of the American Chemical Society*, 2007, **129**, 7510-7511.
5. K. J. Suhr, L. D. Bastatas, Y. Shen, L. A. Mitchell, G. A. Frazier, D. W. Taylor, J. D. Slinker and B. J. Holliday, Phenyl substitution of cationic bis-cyclometalated iridium(iii) complexes for iTMC-LEECs, *Dalton Transactions*, 2016, **45**, 17807-17823.
6. J. Liu, C.-J. Yang, Q.-Y. Cao, M. Xu, J. Wang, H.-N. Peng, W.-F. Tan, X.-X. Lü and X.-C. Gao, Synthesis, crystallography, phosphorescence of platinum complexes coordinated with 2-phenylpyridine and a series of β-diketones, *Inorganica Chimica Acta*, 2009, **362**, 575-579.
7. D. C. Powers, D. Benitez, E. Tkatchouk, W. A. Goddard, III and T. Ritter, Bimetallic Reductive Elimination from Dinuclear Pd(III) Complexes, *Journal of the American Chemical Society*, 2010, **132**, 14092-14103.